ABSTRACT

Geology of the Late Pleistocene Artifact-Bearing Wasiriya Beds at the Nyamita Locality, Rusinga Island, Kenya

Alexander A. Van Plantinga, M.S.

Mentor: Daniel J. Peppe, Ph.D.

This study investigated the sedimentology and stratigraphy of the Late Pleistocene Wasiriya Beds at the Nyamita locality on Rusinga Island, Kenya in northeastern Lake Victoria. Little is yet known about this region during the Pleistocene. This study provides geological context for archaeological research of the stone artifacts in the Wasiriya Beds, for the paleontological work on the fauna of these beds, and for other paleoenvironmental research in these beds. A robust tephrostratigraphic framework was established using diverse statistical methods. Radiocarbon dates confirm a Late Pleistocene age for these deposits. A valley-drainage model was integrated with a facies model to infer their paleoenvironmental history. Sediments suggest a generally sharply alternating wet and dry seasonality. Geological evidence does not suggest that the Lake Victoria region was especially arid just prior to the Last Glacial Maximum. Additional data from the lower Wasiriya Beds could elaborate on their paleoenvironmental significance.

Geology of the Late Pleistocene Artifact-Bearing Wasiriya Beds at the Nyamita Locality, Rusinga Island, Kenya

by

Alexander A. Van Plantinga, B.S.

A Thesis

Approved by the Department of Geology

_____

Steven G. Driese, Ph.D. Chairperson

Submitted to the Graduate Faculty of
Baylor University in Partial Fulfillment of the
Requirements for the Degree
of
Master of Science

Approved by the Thesis Committee

_____
Daniel J. Peppe, Ph.D., Chairperson

_____
Stacy C. Atchley, Ph.D.

_____
Joseph V. Ferraro, Ph.D.

Accepted by the Graduate School
December 2011

_____
J. Larry Lyon, Ph.D., Dean

TABLE OF CONTENTS

LIST OF FIGURES vi

LIST OF TABLES vii

ACKNOWLEDGEMENTS viii

Introduction 9

Human Evolution During the Late Pleistocene 9

Lake Victoria and Late Pleistocene East African Paleoclimate 10

The Wasiriya Beds of Rusinga Island, Kenya 14

Purpose of this Study 18

Study Location 20

CHAPTER TWO 22

Methods 22

Section Measurement and Sampling 22

Tephrostratigraphy 23

Statistical Tests for Tuff Geochemical Equivalence 26

CHAPTER THREE 28

Results and Interpretations 28

Lithostratigraphy 28

Tephrostratigraphy 28

Supplementary Stratigraphic and Geochronological Control 35

Facies and Corresponding Depositional and Diagenetic Interpretations 37

CHAPTER FOUR 53

Discussion 53

Depositional Model and Paleoenvironment 53
Regional Climate Inferred from the Wasiriya Beds 57
Prediction of Archaeological Site Distribution 59
CHAPTER FIVE 61
Conclusions 61
WORKS CITED 62
APPENDICES 63

LIST OF FIGURES

Figure 1 Location of study site 16

Figure 2 A map of the Nyamita locality with points of interest 21

Figure 3 Back-scatter electron (BSE) image of tuff sample 24

Figure 4 Panel of stratigraphic columns 30

Figure 5 Total alkali silica diagram 31

Figure 6 One-way-analyses of elemental oxides by tuff sample 32

Figure 7 Principle Components Analysis (PCA) scatter plot of tuff samples. 33

Figure 8 UPGMA cluster analysis dendrogram 34

Figure 9 Wasiriya Beds facies at Nyamita 38

Figure 10 Structural cross-section of the geological transect at Nyamita 39

Figure 11 Fragment of the AV1006 tufa 40

Figure 12 Tuffaceous silt paleosol deposit at Nyamita 2 45

Figure 13 Tuff sample thin sections 45

Figure 14 Manganese-oxide staining on a ped-surface 52

LIST OF TABLES

Table 1 Nyamita tuff sample means 31

Table 2 MANOVA Hotelling's T^2 pairwise comparison table 33

ACKNOWLEDGMENTS

Thank you to my advisor Dan Peppe, my committee, and all the great faculty and staff in the Baylor Geology department. They put a genuinely friendly face on academics. I couldn't ask for a better graduate program. Thanks to the Baylor Geology grad students for being great friends and classmates. Thanks to my supportive family. I am grateful for funding provided by the Geological Society of America, Baylor Geology, and the Baylor Graduate School, as well as collaborators' funding through National Science Foundation (BCS-1013199 and BCS-1013108), the Leakey Foundation, and the National Geographic Society's Committee for Research and Exploration (8762-10). This work would not be possible without their generous support. Thanks to Christian Tryon, the Rusinga Island researchers, Julian Ogondo, the National Museums of Kenya, and the British Institute in East Africa for facilitating the field research and post-field research. This research was conducted under research permit NCST/5/002/R/576 issued to Christian Tryon and an exploration and excavation license issued by the National Museums of Kenya (NMK). Thanks to Jared Olelo for great field-assistance, and Rusinga residents for being kind and patient. Thanks to Ray Guillemette and Texas A&M University for the probe work, and Spectrum Petrographics for the thin sections. I would like to shout out to J.W.K. Harris and the KFFS alumni.

CHAPTER ONE

Introduction

Human Evolution during the Late Pleistocene

The Late Pleistocene archaeological record between 300 ka and 20 ka is marked by at least two important phenomena: 1) the dispersal of *Homo sapiens* from Africa to Eurasia (Mellars, 2006), and 2) a major shift in stone and other artifact assemblages possibly signaling the emergence of modern human behavior (McBrearty and Brooks, 2000; Klein 2009). Although essentially modern human skeletal morphology emerged by 190,000 ka (McBrearty and Brooks, 2000), the origin of modern human behavior as inferred from the artifacts of the Late Stone Age (LSA) may not have emerged until about 40 ka (Klein, 2000; Klein, 2009). McBrearty and Brooks (2000) contend that the changes in the archaeological record post-dating about 250 ka (such as the emergence of the LSA) are more attributable to additive cultural transmission rather than a punctuated amplification of an adaptive mutation, referred to as a "human revolution," and they suggest that it might have rather been the Early Stone Age-Middle Stone Age (ESA-MSA) transition at about 300-250 ka when modern human behavior evolved.

Artifact diversity during Stone Age transitions may correspond with behavioral, environmental, geographic, and temporal variation, but much more research is needed to characterize the ecological niches and adaptive strategies of the earliest modern humans (Lahr and Foley, 1998; Howell, 1999; McBrearty and Brooks, 2000; Grine et al., 2007; Barham and Mitchell, 2008; Jacobs et al., 2008; Pearson, 2008; Crevecoeur et al., 2009; Gunz et al., 2009; Tishkoff et al., 2009). Throughout the Late Pleistocene, East Africa

was affected by a fluctuating global climate (Trauth et al., 2009). The general correspondence, if any, of early human paleoenvironments with artifacts manufactured is a hypothesis that can be tested with a large volume of data from many archaeological sites spanning Late Pleistocene deposits across East Africa and South Africa (Ambrose and Lorenz, 1990; Eerkens and Lipo, 2005; Banks et al., 2006; McCall, 2007). The consensus amongst archaeologists is that the significance of the African Late Pleistocene archaeological record relies heavily on its paleoenvironmental context.

Lake Victoria and Late Pleistocene East African Paleoclimate

At 263,000 km^2, Lake Victoria is the largest lake in Africa by surface area (Kendall, 1969). It is roughly equidimensional compared to longitudinally elongated East African Rift graben lakes such as Lake Malawi and Lake Tanganyika. Also it is relatively shallow with a maximum depth of 79 m and an average depth of 40 m (Kendall, 1969). The lake is partially fed by the Kagera and Katonga Rivers, and it drains into the White Nile, a tributary of the Nile River along with the Blue Nile. However, 90 % of Lake Victoria's annual water input is from rain within the Lake Victoria basin (~1470 mm/yr); and, of this rain, 70 – 80 % is derived from the lake itself (Beuning et al., 1997; Beuning et al., 2002). Lake Victoria directly contributes ~50 % of total regional rainfall that in turn sustains smaller regional lakes (Flohn and Burkhardt, 1985). The lake occupies the trans-equatorial basin situated in the inter-rift plateau between the eastern and western East African rift-valleys (Kendall, 1969). Little is known about the lake between the time that the basin is hypothesized to have formed at ~400 ka and the Last Glacial Maximum (LGM) at ~20 ka. The lake mainly rests on Precambrian intrusive and metamorphic bedrock with some Tertiary volcanics in the

eastern portion of the basin (Van Couvering, 1972). It has been suggested that the lake formed as western tectonic uplift blocked the westward flowing Kagera and Katonga Rivers, which consequently reversed their flow resulting in back-ponding and eventually the lake (Kendall, 1969; Bishop and Trendall, 1967). Johnson et al. (2000) used seismic reflection data to support this hypothesis of lake-formation and to further hypothesize that the lake experienced desiccation events that occurred approximately every 100 ka, paced by orbital cycles. More research must be performed to elucidate the pre-Holocene history of Lake Victoria, which remains largely unknown (Bishop, 1966; Doornkamp and Temple, 1966; Kendall 1968; Johnson et al., 2000).

Research in the Lake Victoria region can elucidate questions about regional paleoclimatology and evolutionary biology (Johnson et al., 1996; Stager and Johnson, 2008). Arguments have been made that periods of intense climate variability correspond with periods of rapid speciation, though this is difficult to test (Potts, 1998; Maslin and Trauth, 2009; Trauth et al., 2009). For instance, Trauth et al. (2010) describe the amplifier lakes hypothesis as a way to potentially correlate regional species evolution to climate-driven changes in East African lakes. This approach can be taken toward Lake Victoria because, for instance, a hypothetical 60 m drop in modern lake level would shrink Lake Victoria to ~¼ of its current surface area, from 263,000 to 67,400 km^2 (based on bathymetry in Figure 1 from Talbot and Laerdal, 2000). This could drastically alter how the lake functions: as a regional fresh water source; as a barrier to species migration; and as a substitute for potential alternative habitats (wetland, grassland, woodland) that could emerge where the lake recedes.

Ongoing research is deciphering the implications of paleoclimate data from East Africa and integrating those data with larger scale mechanisms of moisture distribution and global models of heat distribution. Moisture distribution is by far the most emphasized factor in East African paleoclimatology. Paleosols in sediment-cores from Lake Victoria and seismic reflection data indicate that the Lake Victoria basin experienced complete desiccation between ~17.5-15.2 ka (Johnson et al., 1996; Talbot and Laerdal, 2000). This paleosol horizon geochronologically corresponds approximately with the onset of northern hemisphere deglaciation after the Last Glacial Maximum (Johnson et al. 1996; Stager and Johnson, 2008). Stager et al. (2011) hypothesize that this arid interval may be the result of polar glacial melt water (Heinrich event 1) that lowered Atlantic sea-surface temperatures, thus weakening oceanic and atmospheric circulation, and diverting moisture from East Africa.

There is also an ongoing debate on the influence of climate change in high- vs. low-latitudes. Revel et al. (2010) examined Nile Delta sedimentary and geochemical successions, and their data support general assumptions that glacial periods correspond with overall greater continental dust flux (especially from the Sahara and Arabian deserts). They inferred two major pluvial periods in the Ethiopian highlands (98-72 ka and 14-8 ka), and additionally inferred two relatively humid periods within the last glacial period in East Africa (60-50 ka and 38-30 ka) that they suggest correspond to major atmospheric increases in methane produced by East African wetlands. Incidentally, Bock et al. (2010) interpreted from hydrogen isotope records that Dansgaard-Oeschger (D-O) warming events 7 and 8 drove high-latitude wetland methane emissions at about 40.1-33.7 ka.

Clement et al. (2004) argued that the tropical hydrologic cycle covaried more directly with precessional signals than polar glacial signals. Trauth et al. (2003) and Trauth et al. (2009) argued that tropical African Pleistocene climate was driven by low-latitude solar insolation variation (on a precessional scale; 23-19 kyr) that resulted in tropical monsoon variability rather than directly covarying with high-latitude glaciation (deMenocal, 2004). Sediment cores from Lakes Naivasha (Trauth et al., 2001), Malawi (Cohen et al., 2007), Tanganyika, and Bosumtwi (Scholz et al., 2007) indicate that East African megadroughts (episodes of regional hyper-aridity) through the Late Pleistocene show poor fidelity with polar glacial variability, but correlate well with monsoonal proxy records. For example, Cohen et al. (2007) inferred that Lake Malawi experienced far more severe aridity during a time-span cross-cutting glacial and inter-glacial intervals (135-90 ka) than during the LGM. However, Brown et al. (2007) note that Lake Malawi appears "out of step with other lake records in East Africa," meaning East African lakes can potentially contradict each other's regional paleoclimate signals. Broecker (2003) suggested that shutdown of the thermohaline circulation (Meridional Atlantic Overturn Circulation (MAOC)) by polar glacial melt-water release drove D-O events that tend to coincide with northward ITCZ migration, depriving Lake Malawi of monsoon rain. Stager et al. (2011) observe that polar glacial melt events coincide with drought in the northern and southern tropics, casting doubt on general assumptions about the response of the ITCZ to polar glacial activity, and suggesting that new thinking is necessary to relate high- and low-latitude climate change.

Others suggest a tropical driver of D-O warming events such as insolation-forced Indian monsoon variability (Clement et al., 2001; Sirocko, 2003; Leuschner and Sirocko,

2003). As part of the Lake Malawi Drilling Project, Brown et al. (2007) determined that signals for Lake Malawi's windy arid time periods not only coincide with D-O events but also precede the onset of D-O events, suggesting that a tropical mechanism could drive high-latitude climate change. However Brown et al.'s (2007) conclusions have come under some criticism for the uncertainty of their radiocarbon age constraints (Garcin, 2008). In agreement with Stager et al. (2011), Tierney et al. (2008) infer from Lake Tanganyika isotope records that Indian Ocean sea surface temperature (SST) variability better correlates with East African Pleistocene paleoclimate variations than assumed ITCZ migration. The Atlantic Ocean and Indian Ocean monsoons apparently interact with each other to shape climate in tropical East Africa (Tierney and Russell, 2007). Future research may elucidate how low-latitude insolation variation over the Indian Ocean and high-latitude insolation variation over the Atlantic Ocean can synergistically affect tropical East African climate. Characterizing and relating intrinsic and extrinsic forcing mechanisms in East African paleoclimate has strong implications for Late Pleistocene archaeology and paleoecology, particularly in the moisture-sensitive Lake Victoria region.

The Wasiriya Beds of Rusinga Island, Kenya

Rusinga Island is part of Kenya's Nyanza Province and is located in the northeastern corner of Lake Victoria at the mouth of Kenya's Kavirondo Gulf (a.k.a. Nyanza Gulf). Rusinga Island has received new interest as an archaeological locality with preliminary dates in artifact- and fossil-bearing deposits of 33-100 ka (Tryon et al., 2010; Tryon et al., in press). Rusinga Island (Figure 1) is known by paleoanthropologists for the type locality of the Miocene ape genus *Proconsul* (Hopwood, 1933; Leakey,

1948). Archaeological, geological, and paleontological work on Rusinga in 2009 and 2010 has uncovered Middle Stone Age Levallois artifacts and cut-marked bone (Tryon et al., 2010; Tryon et al., in press). Rusinga Island is also distinguished for containing extinct Pleistocene fauna (Faith et al., 2010). It was once thought that East African fauna since the late middle Pleistocene was essentially modern (Potts and Deino, 1995). New work suggests, rather, that truly modern animal communities did not emerge until the Holocene (Marean and Gifford Gonzalez, 1991; Marean, 1992; Tryon et al., 2010; Tryon et al., in review; Faith et al., 2010). This has important paleoecological implications for the paleoenvironmental context of human evolution.

The National Museum of Kenya holds artifacts from Rusinga Island that were collected as surface-finds in 1941, and the earliest known published report of artifact-containing deposits on Rusinga Island dates to 1942 (Kent, 1942). The Pleistocene artifact-bearing strata on Rusinga were dubbed the 'Wasiriya Beds' by Pickford and Thomas (1984). The Wasiriya Beds drape over and around the Miocene rock highlands of Rusinga Island and are underlain by eroded and topographically variable indurated Miocene volcaniclastic bedrock from the carbonatite Kisingiri Volcano (Van Couvering, 1972). Pleistocene deposits on Rusinga Island crop out discontinuously over an area < 10 km^2 around the island, ~ 15 to 36 m above modern lake level (Pickford and Thomas, 1984; Pickford, 1986) (Figure 1). The Wasiriya Beds range in thickness from < 5 cm near the shore of Lake Victoria to > 10m near the central highlands of Rusinga Island (Van Couvering, 1972). The Wasiriya Beds have previously been described as poorly stratified clays to silts and coarse sands (Kent, 1942) and stony, clayey soils with lava

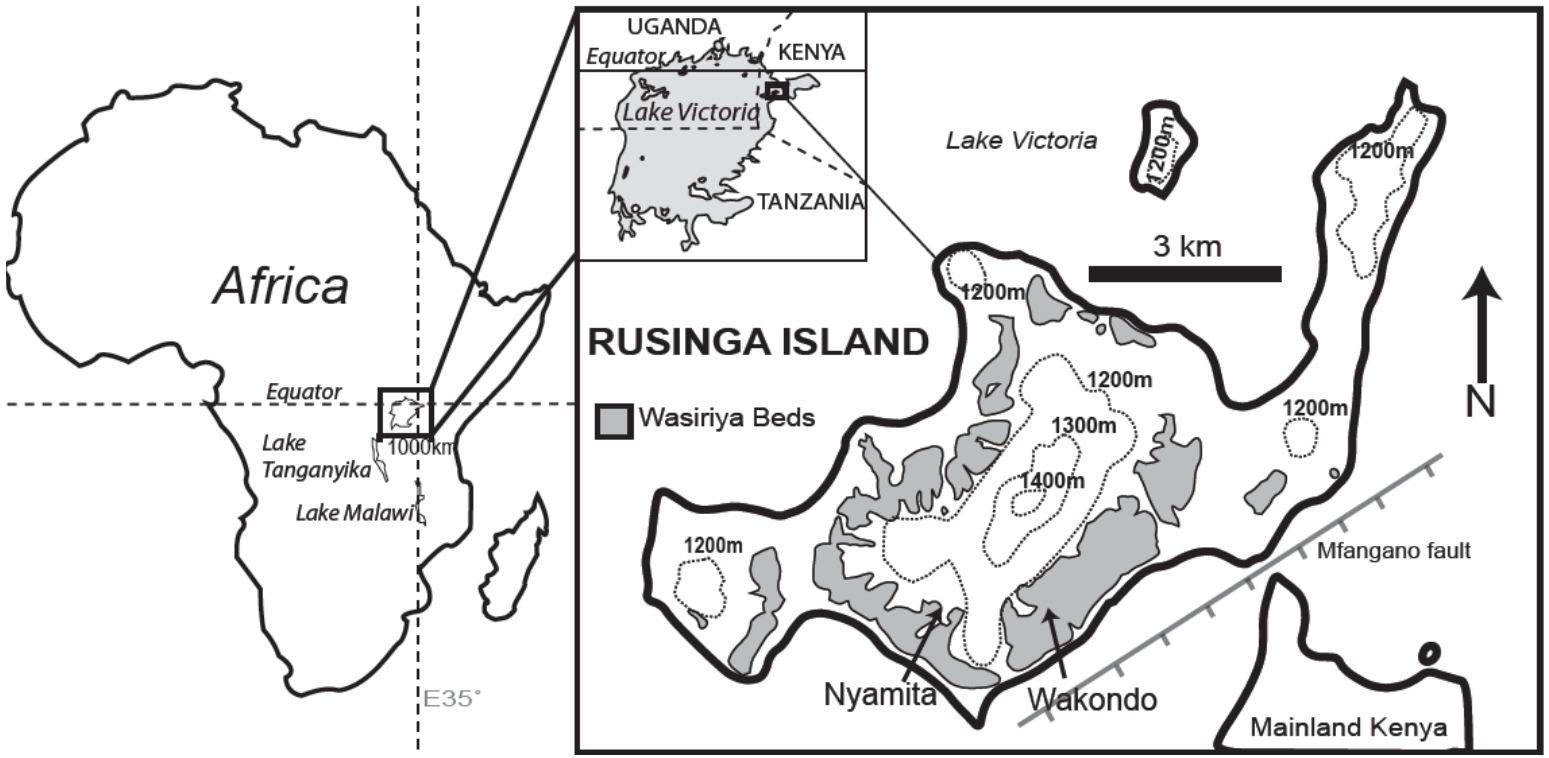

Figure 1 Location of study site.

clasts (Van Couvering, 1972). The Wasiriya Beds were previously interpreted as raised-beach and lacustrine deposits (Van Couvering, 1972; Pickford and Thomas, 1984; Pickford, 1986). Pickford and Thomas (1984) discovered an extinct alcelaphine bovid cranium dubbed *Rusingoryx atopocranion* at the Wakondo locality. An aardvark specimen (*Orycteropus crassidens*) was discovered at Nyamita. The age of the Wasirya Beds has previously been estimated as Middle Pleistocene (based on artifact typology; Kent, 1942; Van Couvering 1971) and as Holocene (based on fossil fauna taxa; Pickford and Thomas, 1984).

More recently Tryon et al. (2010) report finding stone artifacts, cut-marked fossil bone (Wakondo), and they described the first stratigraphic sections from the Wasiriya Beds at the localities Wakondo and Nyamita. They observed silts, sands, and conglomerates with substantial lateral facies variation (such as pedogenic silcrete and carbonate nodules, rootcasts, reworked and airfall tephra deposits, and channel-conglomerates varying from <1 m to several meters wide. Tryon et al. (2010) interpreted the described sections as representing a complex cut-and-fill fluvial environment. They report Late Pleistocene AMS radiocarbon dates of gastropod shells from Nyamita of ~33 – 45 cal ka BP.

Faunal remains such as reedbuck, waterbuck, and hippo, have been found in association with oryx and Grevy's zebra throughout the Wasiriya Beds. The latter species are arid-adapted and rarely range in regions with >500 mm rainfall/year (Tryon et al., 2010; Faith et al., 2010) and isotopic values from pedogenic carbonates (Garrett et al., 2010) indicate that the Wasiriya Beds likely represented a locally wet setting within a broader open arid grassland context (Tryon et al., in press). Fossil fauna in the Wasiriya

Beds include specimens more typical of the modern grasslands east of Lake Victoria, suggesting that the lake was relatively contracted during Wasiriya Beds times (Tryon et al., in press). The gastropod genera from the Wasiriya Beds reported by Pickford and Thomas (1984) (*Limocolaria*, *Burtoa*, *Trochonanina*) and Tryon et al. (2010) (*Limocolaria*) are typical of modern high-elevation grassland/woodland mosaic environments such as Kibwezi Forest, Kenya (Pickford, 1995). *Limocolaria* can be found today in environments as arid as ~300 mm rainfall per year, in which case they aestivate for longer time periods (Haynes and Mead, 1987; Pickford, 1995). The environmental associations of these gastropod taxa vary too widely to be definitive paleoenvironmental indicators on their own. The paleoenvironmental reconstruction thus far contrasts substantially with the modern region's semi-arid to semi-humid climate (500-1000 mm mean annual precipitation) because of the incidence of several arid-adapted species in the Wasiriya Beds (Tryon et al., 2010; Pratt and Gwynne, 1977).

Purpose of this Study

Based on the above, it is reasonable to expect that study of the Wasiriya Beds will pertain to the evolutionary history of human behavior as well as the paleoenvironment of Lake Victoria and more broadly the paleoclimatology of East Africa during the Late Pleistocene (Tryon et al., 2010; Tryon et al., in press). To address these potential implications, a field study of the stratigraphy and sedimentology of Wasiriya Beds at the Nyamita locality was conducted in June 2010. Additionally Wasiriya Bed tuffs were analyzed by electron microprobe to determine if isolated and laterally discontinuous volcanic ash deposits can be chemically correlated. This would enhance the temporal stratigraphic framework that could be used by other researchers for detailed stratigraphic

research in the Wasiriya Beds. Lithofacies were corroborated into a facies model that was used to guide paleoenvironmental interpretation and integrated with the tephrostratigraphic framework for a paleolandscape reconstruction. The geological interpretations were evaluated for consistency with the faunal and isotopic data (Faith et al., 2010; Garrett et al., 2010). Wasiriya Beds geology was evaluated to develop testable hypotheses about archaeological site formation and distribution of artifacts within the Nyamita locality. This study makes a foundational contribution to work in the Wasiriya Beds in that it provides geological, temporal, and paleoenvironmental context for work in the Wasiriya Beds. This work additionally pertains to broader hypotheses about Late Pleistocene paleoclimate in East Africa (Johnson et al., 1996; Talbot and Laerdal, 2000; Trauth et al., 2001; Trauth et al., 2003; deMenocal, 2004; Cohen et al., 2007; Scholz et al., 2007; Tierney and Russell, 2007; Stager and Johnson, 2008; Tierney, 2008; Trauth et al., 2008; Revel et al., 2010; Trauth et al., 2010; Stager et al., 2011).

Here are some specific and also some broader, more open ended questions that this research addresses: Do the Wasiriya Beds contain lacustrine facies? Do the Wasiriya Beds reflect seasonal climate? What might have been the mean annual precipitation? What were the main controls on deposition and erosion? Does the geology of the Wasiriya Beds suggest coupling or of high-latitude and tropical climate? Conversely, does the geology of the Wasiriya Beds suggest that East African lakes are out of step with high-latitude climate - or even that the Lake Victoria region is out of step with other East African lakes? Do the Wasiriya beds show evidence of a major drought, or evidence of the humid periods (60-50 ka and 38-30 ka) inferred by Revel et al. (2006)?

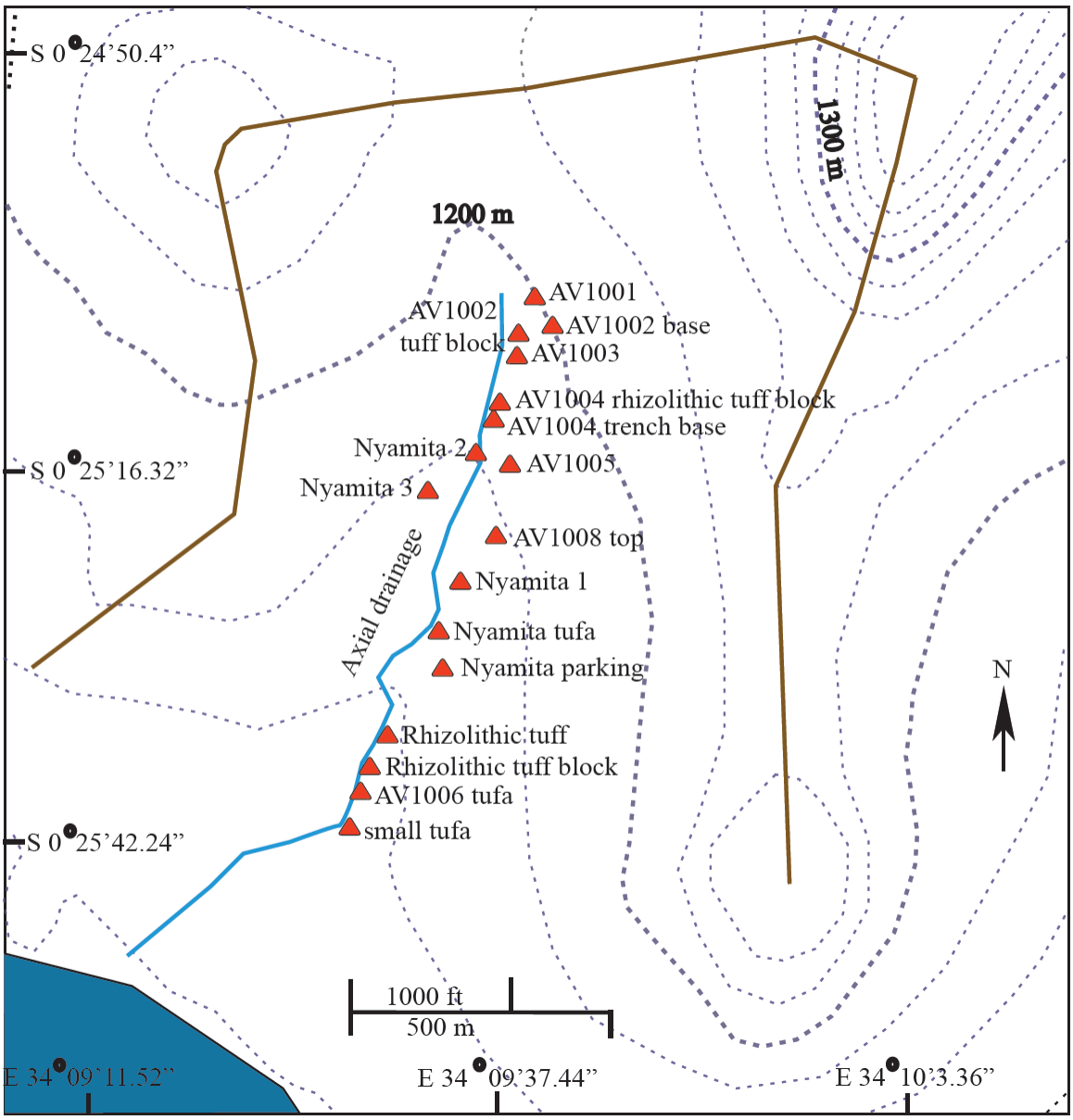

Figure 2 A map of the Nyamita locality with points of interest such as measured sections, tuffs, and tufas. Drainage divides are in brown; the countour interval is 20 m (based on information from Google).

Study Location

This study focuses on a 1 km north-south transect at the Nyamita locality. Nyamita (Figures 1 and 2) is an ideal locality for my main research objectives because it was identified as the locality with the most extensive and numerous Pleistocene exposures. Nyamita is situated in a topographic valley and contains relatively thick (~3-

12 m) deposits of Pleistocene sediment. The valley is carved by a network of modern gulleys. The gulleys combined with variable bedrock antecedent topography produce a steeply undulating modern topography. Tephrostratigraphic methods have produced a stratigraphic framework that contextualizes and constrains the contents of the beds such as lithic artifacts, fossils, and samples for geochemical analyses and dating. Interpretation of Nyamita field-data has led to a depositional model that accounts for the Pleistocene geology at this locality.

CHAPTER TWO

Methods

Section Measurement and Sampling

Rusinga Island was surveyed for Pleistocene deposits in 2009 (Tryon et al. 2010), and in 2010 (Tryon et al., in press). Pleistocene deposits are distinguishable from Miocene bedrock, which tends to be relatively consolidated and distinctively bedded rather than massive. At Nyamita, Miocene bedrock is predominantly composed of red fissile mudstone, agglomerate, and braided channel conglomerate facies (Van Couvering, 1972). Modern alluvium constitutes very little accumulation (< 10 cm) at Nyamita, probably due to the steep topography and lack of anchoring vegetation that causes a modern net sediment loss at Nyamita as with much of the Lake Victoria basin due to grazing and deforestation (Kendall, 1969). Pleistocene deposits were identified as per the lithologic descriptions given by Tryon et al. (2010): by composition, grain size, texture, degree of induration, by the absence of Miocene characteristic facies, by the distinct abundance of calcium carbonate nodules, and by containing Pleistocene-dated gastropods and stone artifacts.

Sections were trenched on gulley walls to expose primary bedding and sedimentary structures. Beds were measured to the nearest centimeter and were described based on lithofacies (composition, color, grain size, sorting, texture, degree of induration, calcareousness, bed contacts and transitions, lateral variability, sedimentary structures, and artifact and fossil content). *In situ* gastropods were collected from several horizons for AMS ^{14}C-radiocarbon dating, which was conducted at the NSF-Arizona

AMS Facility. As tuffaceous deposits were encountered, about 200 gram samples were extracted for tephrostratigraphic correlations and were thin-sectioned for petrographic and electron microprobe analysis.

Tephrostratigraphy

Tephrostratigraphy is a standard method of temporal correlation in paleoanthropology and archaeology (e.g., Feibel, 1999; Tryon et al., 2009). Volcanic ash deposited from an individual volcanic eruption represents a virtually isochronous stratum unless reworked and redeposited (Campisano and Feibel, 2008). Vitric ejecta from an eruption represent the unique chemistry of the melt which varies through time in the magma chamber, and such ejecta tend to be geochemically distinct from one eruption to the next (Feibel, 1999; Sarna-Wojcicki, 2000). Because of these attributes, volcanic ash deposits with minimal diagenetic alteration have provided the means to reliably correlate strata from disparate Wasiriya Bed deposits where field correlations were not possible. It is important to note, however, that tephrostratigraphic correlations are hypotheses only (Feibel, 1999; Brown et al., 2006).

Polished thin sections of the tuffaceous samples were prepared by Spectrum Petrographics Inc., using glass slides (27 x 46 mm), Epotek 301 vacuum impregnation, alumina polish, ground to a thickness of 30 microns. Thin sections were then carbon-coated and optically scanned at the electron microprobe laboratory at Texas A&M University. Geochemical data were collected at Texas A&M on a Cameca SX50 electron microprobe at a setting of 15.0 kV, 10nA, 10 µm beam diameter. On-peak and off-peak times were equal to each other respectively. On-peak times in seconds are as follows: Si (30), Ti (20), Al (30), Fe (20), Mn (20), Mg (40), Ca (30), Na (20), and K (30).

Reference materials for calibration of Na was Albite, Amelia Courthouse, VA, CM Taylor microprobe standard; Forsterite, San Carlos AZ (USNM 111312/44) was used to calibrate analysis of Mg; Rhyolite glass, Yellowstone, WY (USNM 72854, VG568) was used to calibrate analysis of Al and Si; Orthoclase (location unknown), CM Taylor microprobe standard was used to calibrate analysis of K; Anorthite, Great Sitkin Island, AK (USNM 137041) was used to calibrate analysis of Ca; Rutile (location unknown), CM Taylor microprobe standard was used to calibrate analysis of Ti; Spessartine garnet (location unknown), CM Taylor microprobe standard was used to calibrate analysis of Mn; Fayalite, Rockport, MA (USNM 85276) was used to calibrate analysis of Fe. The following secondary standards were used to test the microprobe's performance: synthetic tektite glass (USNM 2213), VG-568 Yellowstone rhyolitic glass (USNM 72854), and Kakanui hornblende (USNM 143965) (Jarosewich et al., 1980). Thin-sections were optically scanned at 4000dpi resolution and the scans were used as templates for electron probe microanalysis (EPMA) point-mapping. Typical grains analyzed by EPMA are shown in Figure 3.

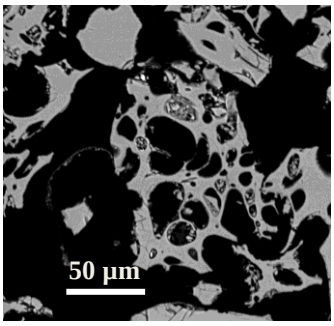

Figure 3 Back-scatter electron (BSE) image of tuff sample AV1004T5A using the Texas A&M University electron microprobe; depicts typical tuff glass shards.

At least ten shards were analyzed per tuff sample (per slide). Elemental oxide abundances were measured for SiO_2, TiO_2, Al_2O_3, FeO, MnO, MgO, CaO, Na_2O, and K_2O as weight percentages (wt. %). The following samples from the field transect of measured sections were analyzed: AV1001T4, AV1002TA, AV1003B, AV1004T3C, AV1004T4C, AV1004T5A, AV1006B, AV1006D. Figure 4 shows the stratigraphic locations of these samples, as well as the proposed correlations, which is why it is in the Results section. A sample previously analyzed by Tryon et al. (2010), CAT09-05, was also analyzed on the Texas A&M University microprobe to monitor the effects of inter-laboratory variation. CAT09-05 was sampled from a Wasiriya Bed deposit at the Wakondo locality (Figure 1) and determined by Tryon et al. (2010) as correlative with the stratigraphically lowest tuff at Nyamita 1, specifically their sample CAT09-01 (Figure 3 in Tryon et al. 2010). The inter-laboratory differences between the Rutgers University EPMA laboratory (Tryon et al., 2010) and the Texas A&M laboratory used in this study were found to be of sufficient magnitude that the data sets from different laboratories are not comparable. This has no effect on the following correlative work which is internally consistent because it uses only the Texas A&M data. Some researchers have emphasized that alkali metals like Na and K can migrate out of a hydrated glass or under a high-intensity electron beam to produce detrimentally variable results and therefore these elements are not reliable indicators of chemical equivalence (Cerling et al., 1985). The low-intensity electron beam used for these analyses produced statistically identical K and Na oxide values in multiple analyses of the same ash grains. Accordingly, electron microprobe K and Na oxide data were used to make the correlations proposed in this study (Hunt and Hill, 1993).

Statistical Tests for Tuff Geochemical Equivalence

Following the methodology of Tryon et al. (2010), samples with totals < 92 % were excluded from statistical tests. This is more robust than the minimum standard (< 90 %) set by Froggatt (1992). Upon data collection, mean elemental oxide percentages and standard deviations were calculated for each tuff sample (summarized in Table 1). Tuff sample means (totals were normalized to 100%) of SiO_2 vs. (K_2O + Na_2O) were plotted on a total alkali silica diagram in accordance with the method of Le Bas (1986) to designate their composition. A variety of methods have been used to establish chemical equivalence of tephra (Campisano and Feibel, 2008; Denton and Pearce, 2008; Lowe et al., 2008; Perkins et al, 1995; Quade and Wynn, 2008; Tryon et al., 2010). Multiple statistical methods were used in this study to determine if they cross-validate each other, potentially increasing confidence in the indicated correlations. For preliminary correlations, univariate one-way analysis plots of elemental oxide percentages were constructed with the statistical software JMP v8.0. Univariate plots can be used to serially compare samples by each elemental oxide to determine which elements are useful for discriminating between tuff samples. Also, univariate plots are less arbitrary than bivariate plots that are commonly used in the literature in that they do not presume specific relationships between individual elemental oxide concentrations (Pollard, 2006). In univariate plots, correlation is based on consistent overlapping of specific elemental oxide means by no more than one standard deviation.

In order to propose correlations in which I can be adequately confident, a multivariate approach was used similar to that used by Tryon et al. (2010). Following the methodology of Tryon et al. (2010) all grain EPMA analyses with totals ≥ 92% were tested with principal components analysis (PCA) using the statistics software JMP v8.0.

The resulting PCA bivariate scatter plot was used to make preliminary multivariate correlations (Figure 8). This was then followed by the use of a MANOVA (multivariate analysis of variance) Hotelling's T^2 pairwise comparison with Bonferroni-corrected values that represent the probability of tuff chemistry centroids being the same, assuming normal sample distributions.

Another multivariate correlative method used was modified Euclidean distances (Perkins et al., 1995; Campisano and Feibel, 2008). This method computes the linear distance between two points in multi-dimensional space in units of standard deviation, using the equation:

$$EDm = \sqrt{\sum_{k=1}^{n}\left[\frac{\left(x_{k1} - x_{k2}\right)^2}{2\sigma_k^2}\right]},$$ (from Perkins et al. 1995; Campisano and Feibel, 2008)

where $xk1$ = the concentration of element xk in tephra sample 1; $xk2$ = the concentration of element xk in tephra sample 2; n = the number of elements used in the comparison; and σk = the standard deviation for analytical precision of element xk. Analytical precision was calculated as the standard deviation of 20 analyses of standard synthetic tektite glass (USNM 2213) because it is theoretically the most homogenous secondary standard of the three used thus its analyses are theoretically most reflective of analytical precision (Jarosewich, 1980). Following the methodology of Campisano and Feibel (2008), the calculated distance values were then used to construct a UPGMA (Unweighted Pair Group Method with Arithmetic mean) cluster analysis dendrogram with the software MSVP v.3.2.

CHAPTER THREE

Results and Interpretations

Lithostratigraphy

The field descriptions of the six measured sections at Nyamita (AV1001, AV1002, AV1003, AV1004, AV1006, and AV1008) are in Appendices 2-7 and represented in the panel diagram, Figure 4. The locations of the measured sections within the Nyamita locality are given in Figure 2. Sections AV1001, AV1002, AV1003, and AV1004 can be generally described as 6-10 m successions whose lower 1/3 is poorly sorted mud, sand, and gravel, which is organized as graded bedding at section AV1002; the middle 1/3 is tuffaceous silt with dense calcium carbonate root and burrow casts, gravel, and gastropods; and the upper 1/3 is predominantly mud with some sand and gravel and carbonate-cemented gravel lenses, gastropods, root and burrow casts, iron- and manganese-oxide staining, and pedogenic carbonate nodules. Section AV1006 contains a large (3.5 m wide) tufa deposit at its base and rhizolithic tuffaceous silt in outcrop or as freestanding blocks upward with gravel lenses interspersed. Section AV1008 extends up-slope northward from the section Nyamita 1 described by Tryon et al. (2010) and consists of mud with gravel lenses.

Tephrostratigraphy

One sight-correlation between tuffs was possible in the field. This was between the sampling location of AV1004T3 in section AV1004 and the sampling location of CAT09-21 from section Nyamita 2 (Tryon et al. 2010), and this is depicted in Figure 4. The resulting EPMA means and standard deviations are given in Table 1. All tuff

samples plot as trachytic on a total alkali silica diagram (Figure 5), but with some variation, as CAT09-05 is nearly phonolitic and AV1004T5A is nearly rhyolitic. Tryon et al. (2010) determined that CAT09-05 is phonolitic by using the Rutgers University EPMA laboratory. This inter-laboratory discrepancy in petrologic classification highlights the effect that inter-laboratory differences in instrumentation and/or methodology can potentially have on interpretation. Until these differences are resolved, ambiguous cases such as sample CAT09-05 should be tentatively regarded as an intermediate of the differing results. Thus CAT09-05 is tentatively trachytic to phonolitic. AV1003TB (n = 11) contains a clearly bimodal population because two grains were consistently chemically dissimilar to all the others, so for statistical analyses, sample AV1003TB was subdivided into populations AV1003TB1 (n = 2) and AV1003TB2 (n = 9). Because AV1003TB1 is only comprised of two shards it was not possible to use it in my tephrostatigraphic correlations. The univariate plots (Figure 6) and the PCA plot (Figure 7) indicate that the sampled tuffs represent three or more distinct eruptions. PCA results suggest that samples AV1001T4, AV1002TA, AV1003TB2, AV1004T3C, AV1004T4C, and AV1006D are correlative and are derived from the same eruption. CAT09-05 and AV1006B may correlate with each other but show weaker overlap. MANOVA results suggest that it is highly improbable that all analyzed tuff samples originated from a single eruption ($p < 0.0001$ for Wilk's lambda, Pillai's trace, and Hotelling-Lawley trace). The Hotelling's T^2 pairwise comparison (Table 2) suggests that

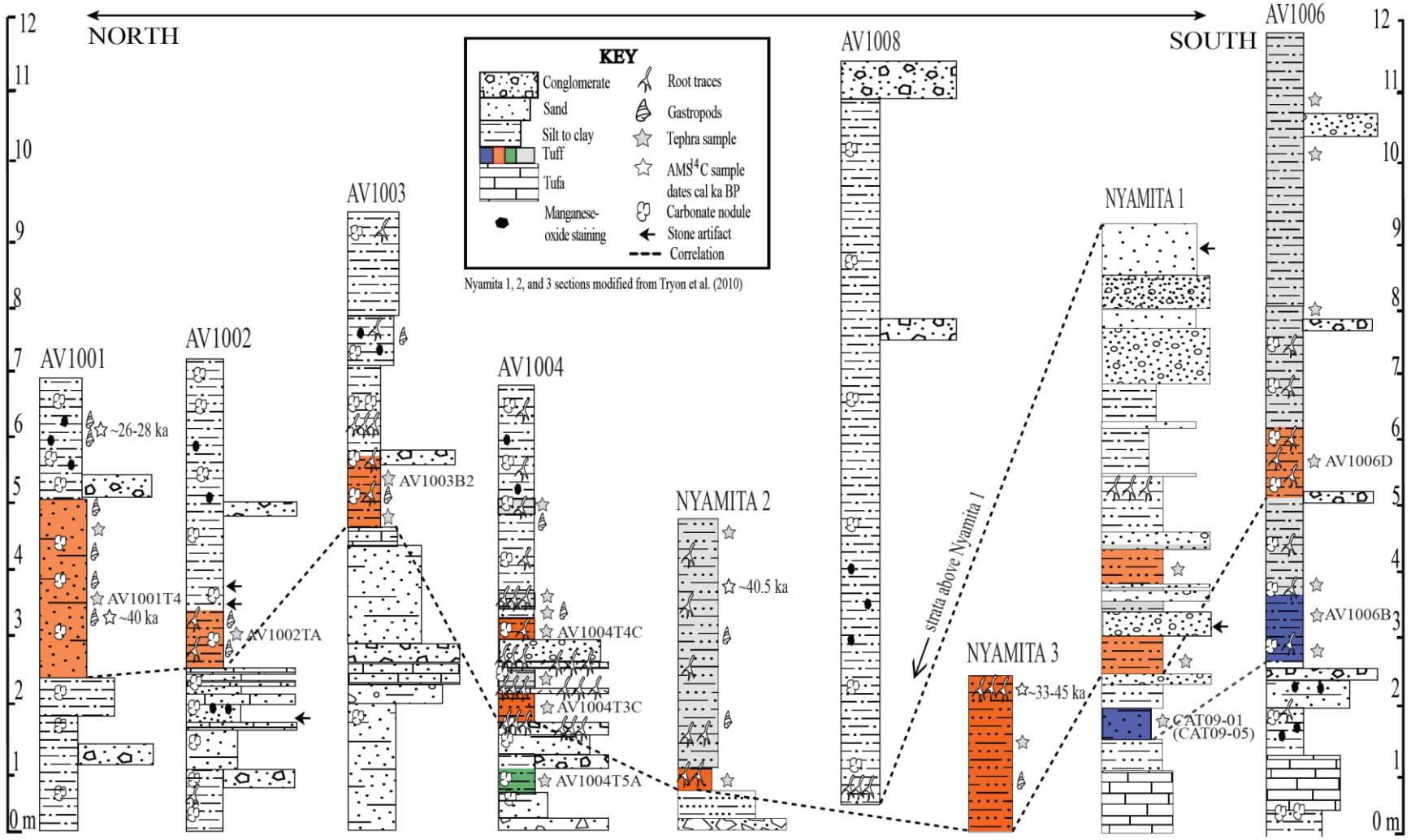

Figure 4 Panel of stratigraphic columns of the Pleistocene deposits at the Nyamita locality, in transect from north to south. Tephrostratigraphically distinct tuffs are color-coded; datum 0 m is the Miocene-Pleistocene contact.

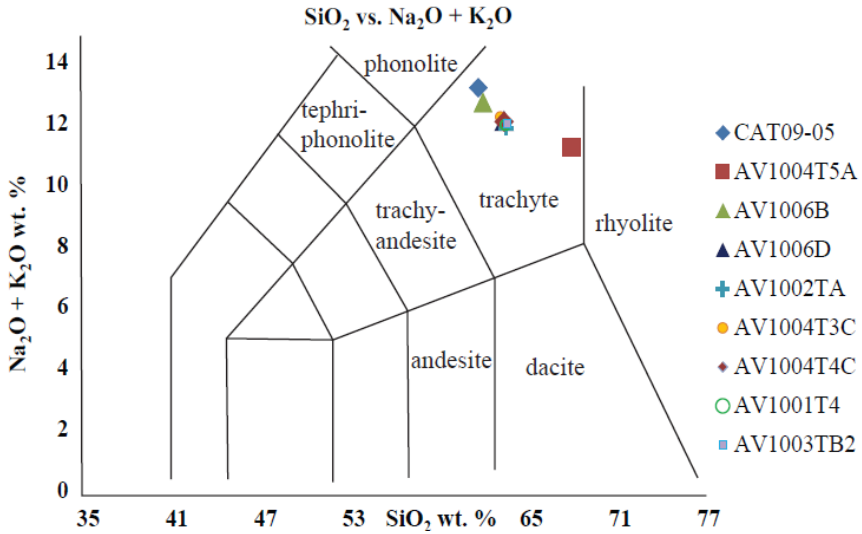

Figure 5 Normalized tuff mean values plotted on a total alkali silica diagram based on Le Bas, 1986.

Table 1 Non-normalized Nyamita tuff sample means and standard deviations for elemental oxide weight % measured by electron microprobe.

Sample	*n*	SiO_2	TiO_2	Al_2O_3	FeO	MnO	MgO	CaO	Na_2O	K_2O	Total
CAT09-05	9	60.28± 0.68	0.59±0.07	15.33±0.14	7.45±0.24	0.30±0.04	0.28±0.01	1.01±0.02	8.21±0.34	4.70±0.14	98.16
AV1004T5A	13	65.11±1.01	0.55±0.08	10.87±0.25	7.77±0.22	0.29±0.05	0.11±0.01	0.66±0.03	6.30±0.31	4.48±0.12	96.15
AV1006B	11	60.10±0.97	0.56±0.08	15.48±0.30	7.28±0.46	0.28±0.04	0.30±0.05	1.03±0.09	7.58±0.83	4.78±0.19	97.38
AV1006D	10	62.00±1.00	0.65±0.12	15.55±0.27	6.45±0.23	0.25±0.02	0.32±0.01	1.11±0.05	6.80±0.18	5.06±0.21	98.18
AV1002TA	13	60.96±0.82	0.60±0.06	15.40±0.26	6.31±0.24	0.26±0.05	0.31±0.02	1.11±0.05	6.58±0.46	4.83±0.27	96.36
AV1004T3C	11	61.60±1.03	0.63±0.24	15.60±0.25	6.42±0.33	0.25±0.04	0.36±0.12	1.18±0.16	6.96±0.30	4.87±0.27	97.87
AV1004T4C	11	61.90±0.93	0.59±0.06	15.37±0.23	6.28±0.10	0.23±0.05	0.32±0.02	1.20±0.07	6.74±0.30	4.92±0.20	96.75
AV1001T4	12	61.16±1.04	0.62±0.07	15.39±0.25	6.32±0.20	0.25±0.05	0.30±0.03	1.11±0.12	6.67±0.42	4.89±0.21	96.70
AV1003TB2	9	61.09±0.73	0.61±0.06	15.37±0.22	6.12±0.26	0.22±0.05	0.30±0.02	1.14±0.05	6.84±0.33	4.72±0.22	96.43

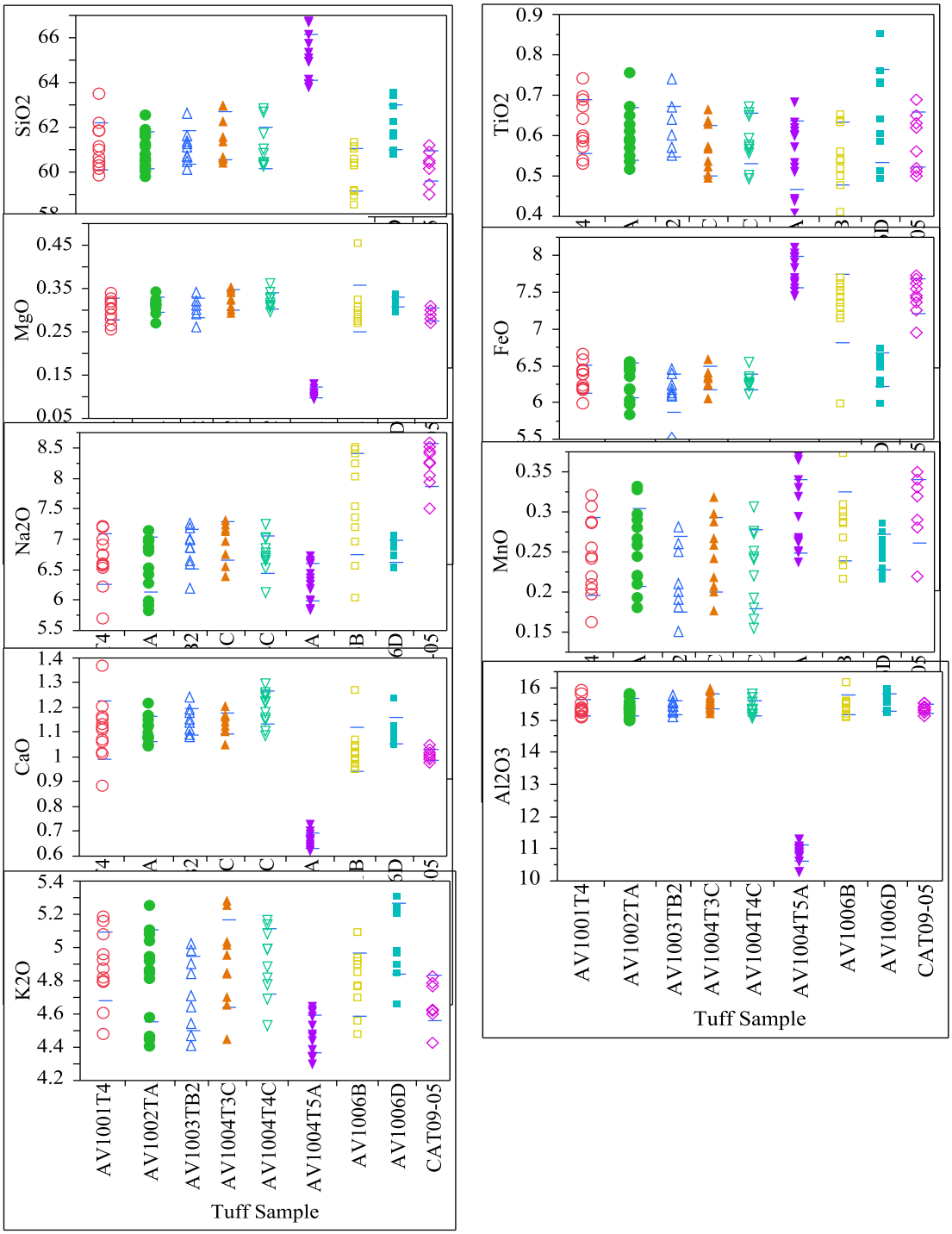

Figure 6 One-way-analyses of elemental oxides by tuff sample. Pairs of bars mark one standard-deviation.

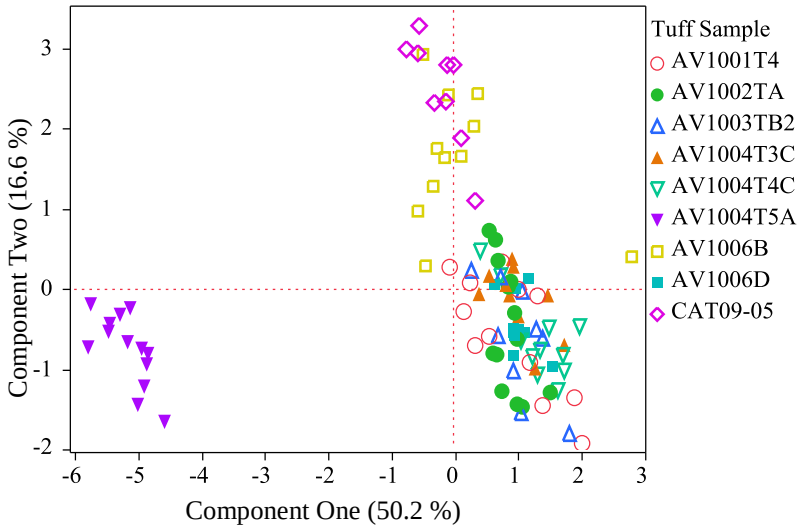

Figure 7 Principle Components Analysis (PCA) scatter plot of tuff samples as indicated, using the two most discriminating components as dimensions. Component percentage is out of total inter-sample variation that the respective axis dimension shows.

Table 2 MANOVA Hotelling's T^2 pairwise comparison table with Bonferroni-corrected values.

AV100↓→	CAT09-05	4T5A	6B	6D	2TA	4T3C	4T4C	1T4
4T5A	0							
6B	1	0						
6D	0	0	0					
2TA	0	0	0	1				
4T3C	0	0	0	1	1			
4T4C	0	0	0	1	1	1		
1T4	0	0	0	1	1	1	1	
3TB2	0	0	0	1	1	1	1	1

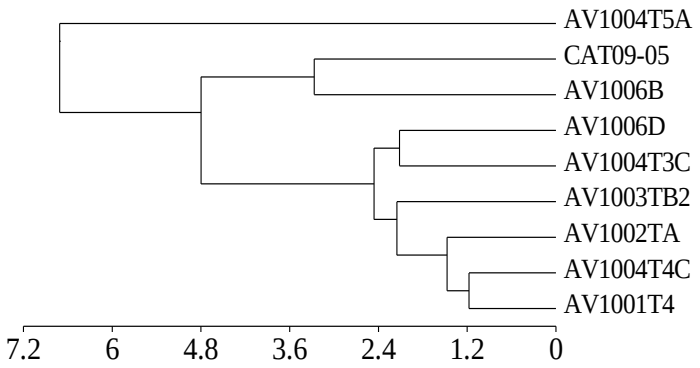

Figure 8 UPGMA cluster analysis dendrogram of non-normalized tuff sample EPMA means generated with the software MVSP v 3.2. The σ*k* values are based on 20 point-analyses of standard synthetic tektite glass (USNM 2213) and reflect the precision of the Texas A&M University Cameca SX50 electron microprobe. Distance is in log(10) units of standard deviation.

CAT09-05 and AV1006B are different from all other tuffs, but not significantly different from each other. Likewise, AV1003TB2, AV1006D, AV1002TA, AV1004T3C, AV1004T4C, and AV1001T4 are all similar to each other, but not to other tuffs. Tuff sample AV1004T5A is different from all other analyzed tuffs. The UPGMA dendrogram of modified Euclidean distances (Figure 8) is consistent with these correlations. The table used to generate this dendrogram is given in Appendix 8.

These results suggest that there is a distinct tuff correlated over hundreds of meters between samples AV1006B from Nyamita and CAT09-05 from Wakondo, which Tryon et al. (2010) correlated with CAT09-01 at Nyamita 1. This deposit appears to be chronologically succeeded by at least one widespread tuff in Nyamita represented by samples AV1003TB2, AV1006D, AV1002TA, AV1004T3C, AV1004T4C, and AV1001T4 (Panel Diagram). There is a third chemically unique tuff is represented by sample AV1004T5A, appearing minimally reworked in hand sample, highly vitric in thin section, and representing an apparently isolated deposit. Accordingly, the use of

tephrostratigraphy has enabled confident correlations of spatially disparate and laterally discontinuous deposits at Nyamita.

Supplementary Stratigraphic and Geochronological Control

It is important to cautiously consider that if cut-and-fill processes acted on the deposits analyzed in this study then conventional laws of superposition do not necessarily apply to them. It is conceivable that the sampled tuffs referred to above might not have conventional stratigraphic utility. Fortunately for the correlations proposed above, the measured section Nyamita 1 in Figure 4 (as modified from Figure 3 in Tryon et al., 2010) contains in succession, and confirms the relative superposition of, the two chemically distinct tuffs for which there are correlations in this study (as portrayed in Figure 4).

Other lithostratigraphic field observations may be confounded by cut-and-fill processes. Because of the limited, patchy, and discontinuous Wasiriya Beds exposures at Nyamita, the apparent superposition of the clayey paleosol facies over the tuffaceous silt facies could not be confirmed by observing one facies directly lying on top of the other. Instead I just consistently observed the clayey paleosol facies adjacent to and elevated relative to the tuffaceous silt. More extensive fieldwork could be conducted to test this hypothetical stratigraphic relationship.

However, AMS radiocarbon age estimates of gastropod shells from strata at Nyamita consistently support my field observations. Note that these dates provide approximate minimum ages for the Wasiriya Beds, since gastropods ingest and assimilate calcium carbonate into their shells. Thus radiocarbon dates from them (genus *Limicolaria*) are often misleadingly old by 0.6-3 kyr (Goodfriend and Stipp, 1983;

Goodfriend, 1987; Haynes and Mead, 1987). The snails probably burrowed into the sediment after deposition, but prior to lithification, to aestivate.

Gastropod sample Snail 2 derived from measured section AV1001 yields an AMS radiocarbon age estimate of 34 690±610 radiocarbon years BP, which is 39 830±914 calendar years BP based on the CalPal-2007$_{Hulu}$ ^{14}C calibration curve of Weninger and Jöris (2008). Tryon et al. (2010) reports similar gastropod age estimates (~33-45 cal ka BP) from the tuffaceous silt deposit in measured section Nyamita 2 (Figure 3 from Tryon et al., 2010). That tuffaceous silt deposit was field-correlated with the tuffaceous silt deposit from AV1004, which was tephrostratigraphically correlated to the tuffaceous silt deposit from which Snail 2 is derived in section AV1001 (using tuff samples AV1001T4, AV1004T3C, and AV1004T4C, Figure 4). Therefore the gastropods dated to ~33-45 cal ka BP from Nyamita 2 (Figure 3; Tryon et al., 2010) came from the same isochronously deposited tuff as Gastropod sample Snail 2 from section AV1001.

Gastropod samples Snail 6 and Snail 7 from AV1001 are derived from the clayey paleosol at the top of the section AV1001. The same clayey paleosol facies caps AV1002, AV1003, and AV1004. Snail 6 yields an AMS radiocarbon age estimate of 22 400±150 radiocarbon years BP, and Snail 7 yields an age estimate of 22 520±160 radiocarbon years BP, which respectively convert to 27 032±537 and 27 238±425 calendar years BP based on the CalPal-2007$_{Hulu}$ ^{14}C calibration curve of Weninger and Jöris (2008). This indicates that the clayey paleosol at the top of the measured sections at Nyamita is distinctly younger (~26-28 cal ka BP) than the adjacent underlying tuffaceous silt deposits (~33-45 cal ka BP), supporting the field observations that the tuffaceous silt deposits are exposed topographically lower than the clayey paleosol deposits in sections

AV1001, AV1002, AV1003, and AV1004. In this instance, cut-and-fill processes have not confounded general assumptions of chronological superposition.

Facies and Corresponding Depositional and Diagenetic Interpretations

Generalized facies from the Wasiriya Beds are distributed at Nyamita as depicted in Figure 9 consist of: 1) tuffaceous silt paleosol; 2) bedded to lenticular rhizomorphic carbonate; 3) conglomerate lenses; 4) graded bedding of calcium carbonate-cemented gravel, sand, and mud; 5) massive mud-supported sand and gravel; 6) clayey non-tuffaceous paleosol; and 7) tufa. The spatial distribution of these facies relative to each other and absolute elevation is shown in Figure 10.

Tufa

There are at least three *in-situ* laminated (Figure 11) limestone deposits at the Nyamita locality (located as shown in Figure 2) which will be referred to here as tufa. Some authors refer to densely laminated terrestrial limestone as travertine (Pentecost, 2005), others as tufa (Andrews, 2005; Matsuoka et al., 2001). While travertine tends to be more consistently identified as densely laminated and a hydrothermal byproduct, tufa can be porous and produced more typically from cold springs. The tufa at the base of AV1006 was the largest observed at Nyamita at 3.5 m wide and 1 m tall as exposed (Figure 9A). The laminations of these spring limestones appear stromatolitic, implying possible algally-mediated calcium carbonate precipitation. Additional work on these deposits is needed to determine their mode of formation.

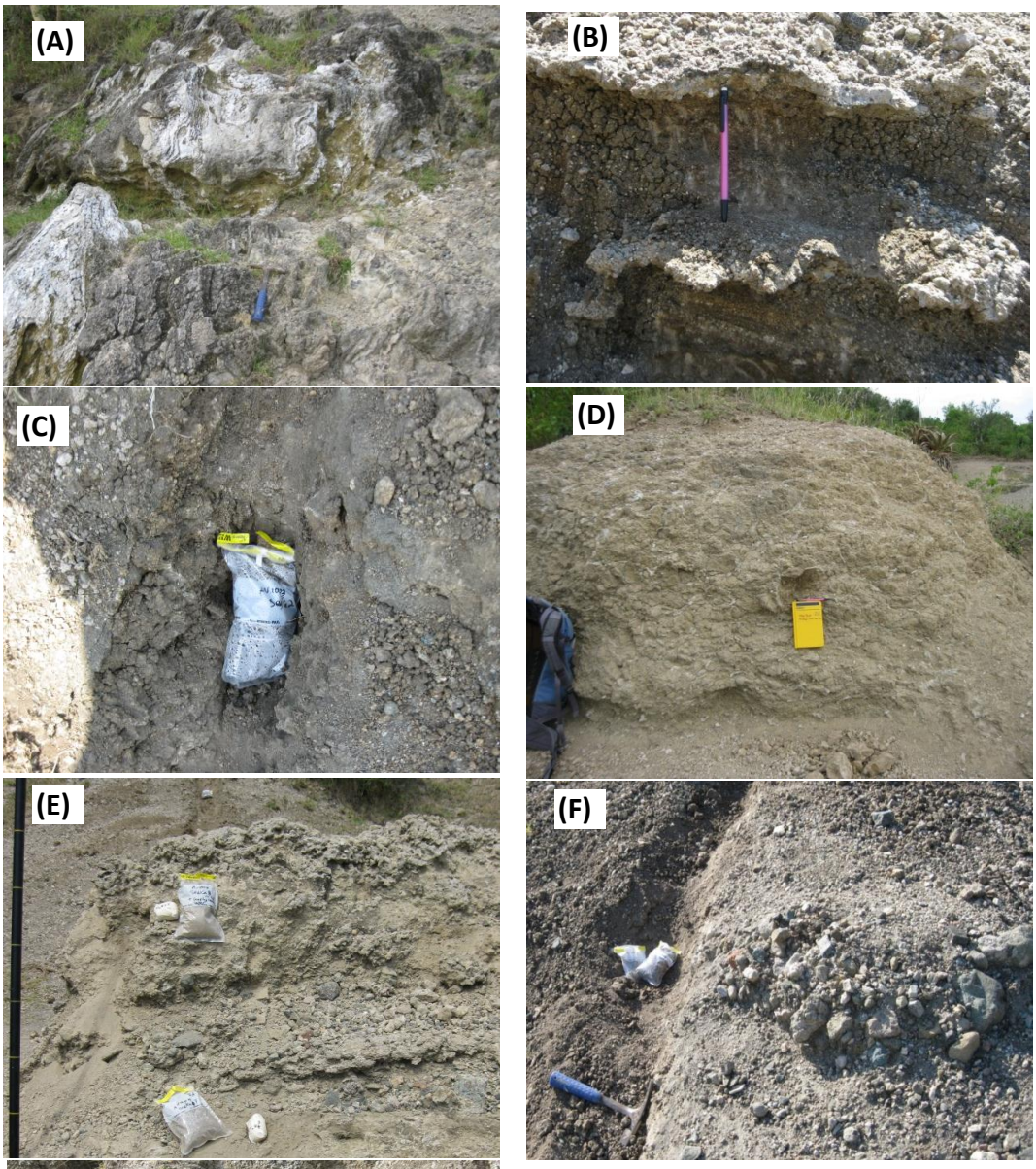

Figure 9 Wasiriya Beds facies at Nyamita, A-F, in the order they are described in the text: A) large tufa at the base of section AV1006; B) graded bedding with carbonate-cemented gravel and cross-bedded sand; pencil = 15 cm long; staff increments = 10 cm, sampling bag = 15 cm long; C) massive, poorly-sorted mud, sand, and gravel; D) rhizolithic tuffaceous silt paleosol block, in section AV1006; notebook = 20 cm tall; E) carbonate rhizolithic lenses in AV1004 tuffaceous silt block; F) conglomerate lens; hammer = 28 cm long; G) clayey paleosol.

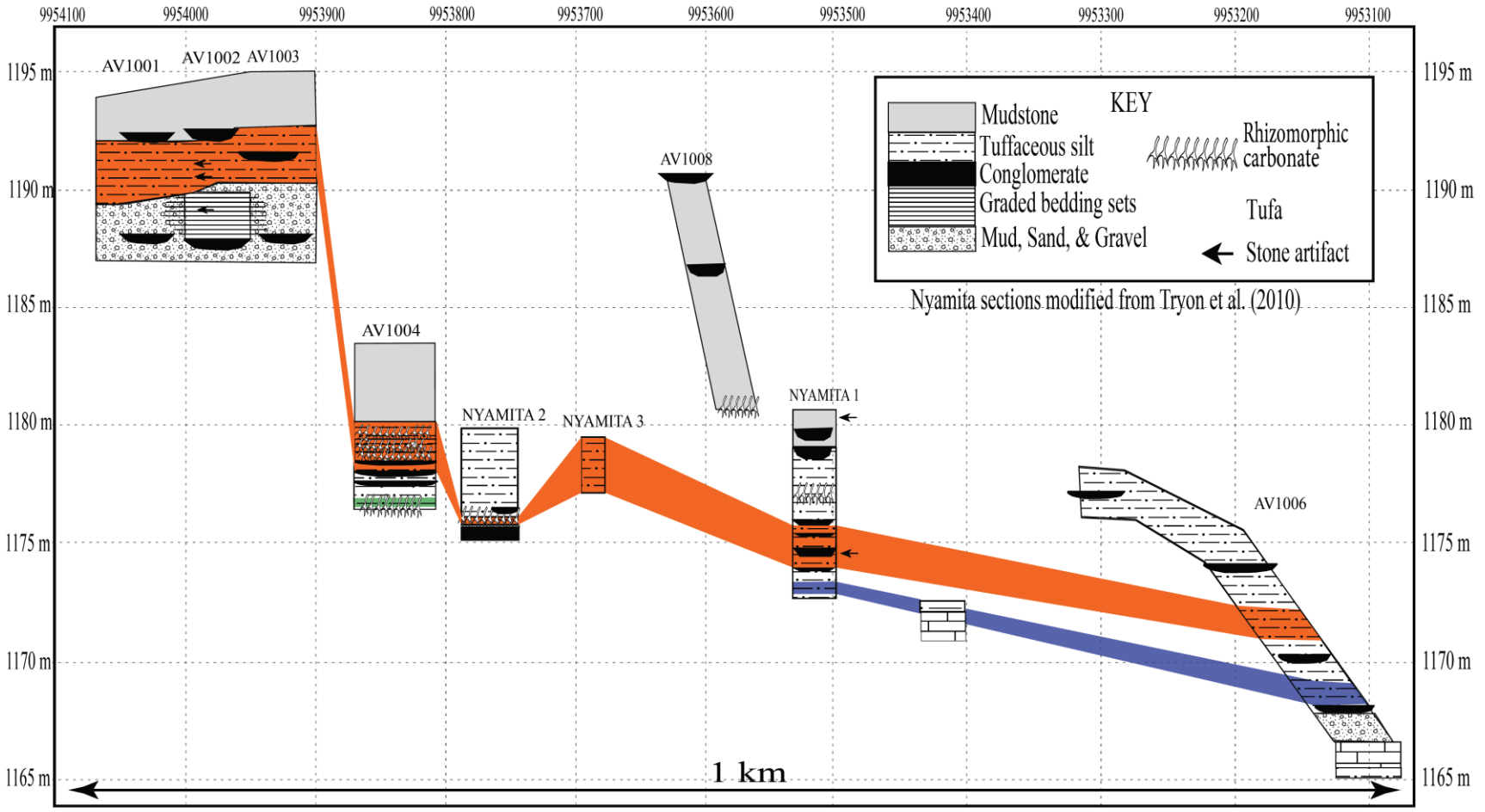

Figure 10 Structural cross-section of the geological transect at Nyamita, spatially relating the described sections and the distribution of facies as per their designations in the text. Vertical units are in relative meters above sea level, which is the topographic datum. Here the viewer's perspective is from the west looking east, with horizontal units in UTM UPS latitude using the datum ARC 1960 36 M. Tuff correlations are depicted to illustrate approximately isochronous paleolandscape surfaces, with each color representing a chemically distinct population of vitric grains.

Figure 11 Example of primary laminations and secondary precipitate in a fragment of the AV1006 tufa; scale increments are 1 mm.

Hippo fossils have been discovered at surface and within the Nyamita 1 section (the uppermost artifact/fossil symbol in Figure 4). Tufa associated with semi-aquatic vertebrate fossils strongly supports the existence of an enduring water source on the landscape during earlier Wasiriya Beds times. The tufa from Nyamita 1 and AV1006 (Figure 4) underlie a correlated tephra deposit (samples AV1006B and CAT09-05, which correlates with CAT09-01), preceding the deposition of the most widespread correlated tuff. In Nyamita there is a modern active spring which feeds a stream channel and a wetland that is east-adjacent to the section Nyamita 1 (Figure 2). This modern environment may be similar to the environment penecontemporaneous with the ancient tufa deposits. The alkalinity of the spring water was logically high, so potassium feldspar precipitate and illitized clay is expected in the sediment associated with the tufas (Hay et al., 1986).

Spring-associated wetland facies are usually comprised of fine, muddy, organic-rich, gleyed sediment (Ashley et al., 2002). No such characteristic wetland facies were observed preserved in the Wasiriya Beds at Nyamita. This could be due to periodic desiccation, oxidation, and/or obliteration of spring-affected environments, depending on rates of sediment controls. Because wetland environments would most likely be situated

at topographic lows and close to the axial drainage such environments would be highly susceptible to fluvial reworking. No direct evidence was found that would suggest there was spring activity during upper (<30 ka) Wasiriya Beds times like in the capping clayey paleosol, although it was possible. Given the size of the valley that comprises Nyamita's watershed (Figure 2), spring discharged likely closely depended on local pluvial input, barring hydrologic conduits like fault and fracture systems that cross drainage divides. Regional climate variation may be directly reflected in tufa chemical composition, such as by constructing an isotope chronology across laminations (Matsuoka et al., 2001; Andrews, 2005).

Graded-Bedding

Successively stacked graded deposits of gravel, sand, and mud, are a distinct facies in Nyamita, though they only occur in section AV1002 (Figure 9B). The graded beds are laterally discontinuous (up to 2 m across). The sand is laminated to low-angle-cross-bedded, scoured by fine gravel (grain size <3 cm) in places, and contains some mud lithoclasts. The very fine to very coarse sand grains are sub-round to sub-angular, heterolithic, and poorly sorted. This suggests close proximity to its source, somewhere within the Nyamita valley or from the highlands directly adjacent to the valley. The capping mud layers are less than 5 cm thick overlaying the sand and underlying the gravel of another graded deposit. There is manganese oxide staining in both the mud layers and in the clay matrix of the sediment underlying the graded bedding interval. The graded deposits bear some of the few recognized fluvial bedding structures in the Wasiriya Beds at Nyamita, other than conglomerate lenses.

Preservation of several graded beds in succession indicates a repetitive deposition under basically the same conditions from one graded deposit to the next. These deposits probably formed when an upslope channel experienced multiple successive pulses of sedimentation from pluvial runoff events, where overland flow funneled high sediment yields into a particular former channel. High sedimentation at this section suggests an abundance of sand upslope on the paleolandscape with little vegetation to retain the sediment (Harvey, 1989), or perhaps a sudden slope-collapse. The formation of a pre-existing channel required substantial erosion at this location just preceding the interval of high-sedimentation that produced the graded beds. Such a stark shift in local depositional regime could represent a temporarily intense rainy phase in an otherwise lengthy arid time period (Pederson et al., 2000; Smith, 1994). In alluvial fan systems, sheet sands can represent abrupt shifts from high to low gradient on the hillslope, suggesting that these deposits occurred at such a place. If the graded beds do not signal a significant climate shift it could be that these deposits were common throughout Wasiriya Beds deposition but rarely preserved due to subsequent bioturbation.

If we assume the manganese oxide staining is penecontemporaneous with the graded deposits, then it suggests the presence of organic matter whose decomposition products can liberate sedimentary manganese (Hem 1964; Mount and Cohen, 1984). This is suggestive of slope denudation coincident with sedimentation, causing a major flux in sedimentary organic matter. Carbonate cementation likely occurred from vadose fluid solute concentration, suggesting the water table fluctuated sharply and frequently in this interval.

In summary, the graded bedding probably occurred at the foot of a slope and may represent a shift from arid/erosional/degradational conditions to rainy/depositional/aggradational conditions and the filling of accommodation space at Nyamita. Such an anomalously rainy interval could be as short as one year, infinitesimal in geologic terms. AV1001 is on the other side of the current modern gulley wall from AV1002, so lateral variability can be evaluated. The deposit in AV1001 that corresponds with the graded deposits in AV1002 is the massive, poorly-sorted mud, sand, and gravel facies.

Poorly-Sorted Mud, Sand, and Gravel

This facies (Figure 9C) is mostly poorly-sorted mud, sand, and gravel, and contains abundant rootlet casts which are evidence of pedogenesis. This facies is the lateral equivalent of the graded bedding facies (Figure 10), interpreted as the distal channel or floodplain corresponding to the fluvial channel in which the graded beds formed during a short rainy timespan that interrupted a longer arid interval. Any bedding structures they contained were obliterated. This facies generally underlies the tuffaceous silt paleosols facies, and is definitely present at the bases of sections AV1001, AV1002, and AV1003. The other measured sections contain gravel and sand at their basal Miocene contacts.

Tuffaceous Silt Paleosol

Tuffaceous silt at Nyamita generally appears as tan to buff colored (2.5Y 5/2, 10YR 7/2, 10YR 5/3) and occasionally gray (GLEY1 6/1). Deposits of this facies exist in every measured section. This sediment is most conspicuous in the form of tuffaceous silt blocks (0.5–4 m thick, 0.5-5 m across) but also exists in pockets and lenses stratified

by clay deposits such as in section AV1001. Generally, the tuffaceous silt is more consolidated when it appears more reworked. When least reworked (pockets of GLEY1 6/1) it is virtually totally unconsolidated and turns to fine silt in hand sample that is easily suspended in the wind. More diagenetically altered tuffaceous silt is more argillaceous (more cohesive) and infiltrated with carbonate root and burrow casts that may provide additional structural integrity for deposits. The thickest deposit of this facies, in section Nyamita 2 (Tryon et al., 2010), shown in Figure 12, has the greatest density of vertical root and burrow casts and gastropods. Authigenic clay in this facies probably derives partially from devitrified tuff.

Tuffaceous silt in Nyamita originated as extra-basinal volcanic ash airfall followed by redepositional and diagenetic processes. The tuff probably became concentrated in the Nyamita locality valley bottom, along the axial drainage by colluvial and alluvial transport. Matrix-supported gravel in these deposits suggests it was transported by debris flow. This facies was apparently preserved by two main mechanisms. Less diagenetically altered tuffaceous silt exists in pockets protectively stratified by calcareous barriers, such as calcified root mats and carbonate-cemented conglomerate lenses. Sustained subaerial exposure and landscape stability are indicated in these deposits by pedogenic features such as abundant and sometimes very dense root and burrow traces (Figures 9E, 13A, and13) and pedogenic carbonate nodules (Figure 12C). Tuffaceous silt blocks at Nyamita 2 (Figure 12) and AV1006 (Figure 9D) contain vertical and horizontal straight unbranching root/burrow casts and randomly oriented rootlets (<2mm diameter) (Figure 12A). The complex horizontal branching indurated

Figure 12 Measured section Nyamita 2 (Tryon et al., 2010), the thickest and most extensive tuffaceous silt paleosol deposit at Nyamita, notebook = 20 cm tall.

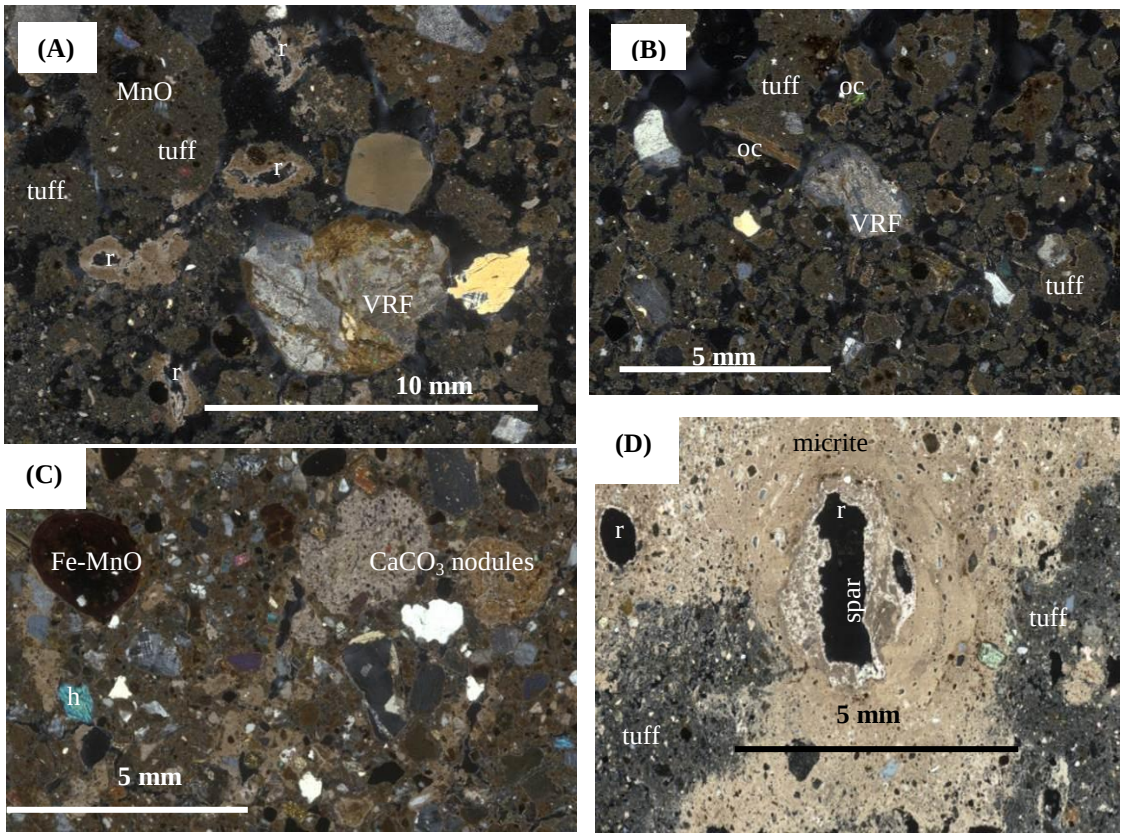

Figure 13 A) tuff sample AV1002TB: diverse tuffaceous paleosol constituents; B) Un-oriented view of tuff sample AV1006D, with oriented clay coating tuffaceous aggregates; C) tuff sample AV1004T1, with pedogenic nodules; D) tuff sample AV1004T4C, showing stark juxtaposition of a calcareous root cast cross-section and vitric tuff; r = root trace, MnO = manganese oxide staining, VRF = volcanic rock fragment, ic = illuviated clay, Fe-MnO = iron-manganese nodule, h = hornblende.

carbonate lenses at section AV1004 are subdivided out as a separate facies described below. The presence of long (> 20 cm) vertical root/burrow casts is indicative of a vadose zone and some degree of soil drainage (Mount and Cohen, 1984). The tuffaceous silt deposits mostly lack characteristics suggestive of soil maturity such as distinct horizonation, ped structure, or extensive tuff devitrification to clay (in which case it would be a different facies such as the clayey paleosol facies). I generally interpret this facies as an incipient paleosol. Gravel lenses within this facies imply occasional fluvial scouring, concurrent with the hypothetical colluvial origin of the tuffaceous silt deposits. Relict bedding structures in the tuffaceous silt are not visible. Presently existing deposits were obviously not fluvially obliterated so they logically represent stable points on the paleolandscape at Nyamita. It is reasonable to infer that deposits of this facies were not subaerially exposed long enough for extensive pedogenesis to occur. How this is conceivable given the radiocarbon ages derived from the tuffaceous silt deposits is discussed below.

Authigenic micritic calcite (Figure 13D) is evidence that these deposits were part of the vadose zone and were hydrologically contiguous with a larger body of sediment/rock. To produce the carbonate burrow and root casts water flowing through this sediment/rock body dissolved calcium carbonate and then evaporated and precipitated it along surrounding pore-space. The primary limestone source of all pedogenic calcium carbonate in the Wasiriya Beds was probably ultimately the Miocene carbonatite volcaniclastic bedrock.

Given the thermodynamic instability of volcanic glass at the Earth's surface, the high surface area of volcanic ash, and its tendency to dissolve in alkaline solution

(Lofgren, 1971), it is peculiar that the tuffaceous silt deposits simultaneously acted as calcareous soils and retain a significant vitric ash component. Not only that, but penecontemporaneous to diagenetic features suggestive of vadose water infiltration (e.g. calcified root mats) are especially difficult to reconcile with the extensively preserved volcanic glass. At Nyamita, volcanic ash is often physically in contact with authigenic calcium carbonate (Figure 13D). Alkaline ground water probably flushed through these sediments numerous times but on what basis is unclear. Clearly some devitrification has occurred producing clay (e.g. Figures 13A, B, and C). However, preserved vitric ash can be found in these deposits, either as a component of homogenized insipient paleosol (AV1002 of AV1006 block), or sometimes resembling clods of unmixed flour in cake batter as in the tuffaceous silt block in section AV1004 (Figure 9F). The tuffaceous silt deposits suggest alternating repetitive infiltration and drying of the vadose zone. Perhaps authigenic clay and calcite mineral deposition protected adjacent tuff from whole-sale devitrification by vadose water. Regardless of the exact mechanism of glass preservation, preserved glass suggests these deposits were only sporadically moist, and points to distinct alternating wet and dry conditions such as seasonal monsoons similar to the East Africa's modern seasonal regime.

For interpreting observations from currently subaerially exposed tuffaceous silt deposits (e.g. Figure 9D), modern overprinting is a serious consideration because observed pedogenic attributes could be approximately modern. For instance, the exposed rhizolithic tuffaceous silt block in AV1006 contains weak blocky ped structure. Additionally, the thin section AV1006D (Figure 13B), from this deposit, contains highly birefringent bands of clay with sweeping extinction. These features are interpreted as

illuviated clay from the process of clay translocation down-profile by rain water. However, given that this observation derives from what is now an entirely subaerially exposed sediment body, this attribute of pedogenic maturity may be a modern artifact (regardless of how deeply one digs). The rhizolithic tuff block in section AV1004 is subaerially exposed, however it is capped by a rhizomorphic carbonate lens and thus the tuffaceous silt underneath this caprock is preserved.

Because the calibrated radiocarbon age estimates of ~33 – 45 cal ka BP for these deposits are derived from presumably burrowed gastropods, pedogenic attributes of this facies are potentially as old or older than these absolute dates, with some caution as noted above. A >10 ka duration of bioturbation as a soil is difficult reconcile with this facies' pedologic immaturity, mainly the weak ped structure and the vitric tuff preservation suggestive of rapid burial (Fuente et al., 2000; Gutierrez-Castorena et al., 2007). Perhaps the thick tuffaceous silt deposits that remain today were buried, re-exposed, and reburied. Abundant channel conglomerate lenses within these and stratifying deposits suggest there was active cut-and-fill activity following the burial of the major isochronous tuffaceous silt deposits. Such processes in a dynamic paleoenvironmental interval could conceivably bury, re-expose, and rebury the tuffaceous silt deposits.

Lenticular Rhizomorphic Carbonate

The calcareous rhizomorphic facies is expressed most distinctly in the AV1004 tuffaceous silt block (Figure 9E). This facies occurs as indurated calcium carbonate deposits, 10-20 cm thick, comprising masses of amorphous to horizontally branching casts 2-3 cm in diameter. This facies was generally observed overlying either conglomerate facies or bedrock, or stratified by tuffaceous silt. Mount and Cohen (1984)

classify horizontal root mats as associated with poorly drained shallow littoral facies lacking vadose conditions, reflecting root mats of aquatic macrophytes and coastal grasses. Semeniuk and Meagher (1981) and Mount and Cohen (1984) describe vadose zone processes that account well for this facies. Calcareous mats of root casts probably formed at seasonally water-logged points on the landscape, mainly places with shallow depth to impermeable sediment/rock (< 4 m). Vegetation colonized these locations and produced dense root mats in the substrate. Then calcite from saturated vadose water precipitated around roots, remaining as cavities in the sediment after death and decay of the original plant matter.

Subsequently the hollow cavities became conduits for vadose water, and diagenetic fluid precipitates accreted and produced solid root and root mat casts. The AV1004 tuff block exhibits successive lenses of this facies, indicating that multiple successive episodes of sediment accumulation and plant rooting occurred at that particular point on the paleolandscape. The stratigraphic evidence at section AV1004 implies a generally more elevated Late Pleistocene paleotopography than present-day. Thus the landscape was aggradational during the time contemporaneous with the widespread tuff deposit (tuffs in orange in Figures 4 and 10).

Lenticular Channel Conglomerates

Gravel lenses (Figure 9F) in the Wasiriya Beds at Nyamita are virtually all polymictic, clast-supported, have random clast-orientation, and do not show consistent sorting by roundness or sphericity. Gravel lens clasts were as large as 25 cm in maximal dimension. Conglomerates occur in tuffaceous silt facies, graded-bedding facies, and clay-dominated facies, indicating that the essential factors of conglomerate formation are

present throughout the depositional interval at Nyamita. These factors are: climate, gradient, sediment supply, and channel dimensions. The Nyamita valley has steep eroding walls that shallow toward the axial drainage. Modern tropical East Africa typically experiences bimodal monsoon and dry seasons but this wasn't necessarily the case in the Pleistocene.

Gravel lenses are interpreted as gulley channel-lag. As logical a proxy of incisement and gullying, the conglomerates signal powerful fluvial currents from torrential rainstorms. Channels formed when erosion outpaced sedimentation. Accumulation of cobbles in channels effectively armored them and attenuated erosion (Beaty, 1959). Conglomerate lenses approximate the width of such channels and range from 0.5 to 2.5 m wide. Some mud-dominated deposits with poorly-sorted sand and gravel clasts are more consistent with liquefied debris flow deposits, but could also be pedogenically reworked fluvial deposits. Bertran et al. (1997) note that fabric patterns cannot be used independently as diagnostic criteria for specific processes (i.e. debris flow versus grain flow), even though these deposits are still sedimentologically informative. The conglomerate lenses show penecontemporaneous carbonate cementation probably from a falling water table.

Clay Paleosol (Non-Tuffaceous)

This facies (Figure 9G) is the capping lithology for sections AV1001, AV1002, AV1003, and AV1004. This facies did not contain bedding indicative of fluvial deposition, although this is still a possibility, since bioturbation clearly evident in this facies would have obliterated primary sedimentary structures. Likewise, the clay may have gradually, additively accumulated to produce this facies. Matrix-supported gravel

clasts distributed throughout this facies may indicate that this facies accumulated from debris-flow, however, a more likely explanation is that bioturbation distributed the gravel through the soil profile. It is unclear how the Rusinga Island highland sediment sources would produce so much clay, which is why I suspect that this facies is extensively devitrified tuff. Future research can evaluate this hypothesis by determining if the clay mineralogy is illite, smectite, or zeolite (de la Fuente et al., 2000). The significance of a tuffaceous origin is that a hypothetical high rate of chemical weathering would be indicative of humid climate.

This facies generally contains carbonate rhizoliths, gastropods, and black manganese-oxide stains but otherwise contain no apparent bedding structures. Tiny multi-directional rootlet casts (< 2 mm diameter) were observed in this facies (Figures 14 and 15). The clay has crumbly, blocky ped-structure, is distinctly darker (Munsell color 10 YR 4/2-3/2) than other facies, and it lacks a substantial tuffaceous component. This facies could record an interval of relative moisture abundance a stable landscape. It is a more mature paleosol than the tuffaceous silt paleosol deposits, suggesting a longer duration of subaerial exposure. Since the clayey paleosol deposits rest at the top of the northernmost and highest stratigraphic sections, they represent the highest and latest preserved evidence of aggradation and accommodation-space fill in the Wasiriya Beds at Nyamita. Thus this facies is suggestive of a floodplain terrace 5-10 m above the modern valley bottom. Gastropods probably burrowed to aestivate during times when the sediment was not water-logged such as during the dry season if such a concept applied. AMS radiocarbon gastropod ages from this facies in AV1001 are about ~26-28 cal ka BP (Figure 4). This coincides with the Last Glacial Maximum, but this is a minimum age

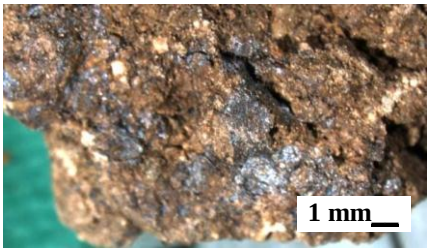

Figure 14 Manganese-oxide staining on a ped-surface from AV1001, at 570 cm height.

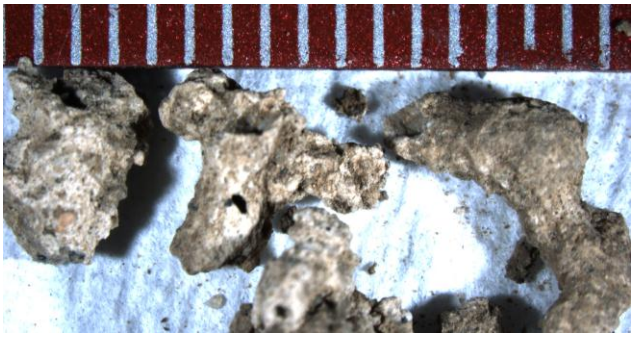

Figure 15 Fine multidirectional branching rootlet casts from the clayey paleosol capping section AV1004 at 590 cm; scale is in mm.

estimate and the clayey paleosol deposits could be several thousand years older. Observed manganese oxide staining (Figure 14) could have precipitated in close association with decaying root matter (Hem 1964; Mount and Cohen, 1984). The high Mn content and presence of fine branching rootlets (Figure 15) suggests that these deposits resided within the zone of mixing between the phreatic and vadose zones, or the Mn precipitation resulted from substantial vegetation denudation on the landscape and consequent dissolved sedimentary organic matter flux. This generally implies a fluctuating water table several meters higher than the modern valley bottom at a time when the Nyamita was substantially vegetated. The conglomerate lenses in this facies (Figure 4 and Figure 10) could be penecontemporaneous or much younger, from subsequent gullying.

CHAPTER FOUR

Discussion

Depositional Model and Paleoenvironment

After a virtually exhaustive search during the 2010 field season, no lacustrine facies were found in the Wasiriya Beds. The Pleistocene deposits at Nyamita are valley-pediment, channel, and hill-slope deposits, so I will use a valley-drainage depositional model to interpret them. Tucker and Slingerland (1997) offer a valley-drainage model that focuses on the variable of climate, which in turn puts focus on rates of hillslope versus channel transport. Theoretically the valley hillslope continuously physically and chemically weathers to develop a mantle of regolith that overland flow colluvially transports to a channel. Tucker and Slingerland (1997) conclude that distribution of precipitation through time, such as frequency and intensity storm events, is a far better correlate with sedimentation regime than mean precipitation. Storm intensity corresponds to runoff intensity and denudation rate such that a shift toward humid rainy conditions is expected to have punctuated high, then rapidly diminishing, denudation and sedimentation rates. When the available mantle of regolith is exhausted from the hillslope, the sedimentation rate declines toward a state of net erosion and channel incisement throughout the valley as the rain continues. Thus the valley-drainage model has utility for evaluating my hypothesis that the Wasiriya Beds at Nyamita reflect penecontemporaneous climate variation.

Since faunal and pedogenic stable isotope evidence suggests an overall semi-arid paleoenvironment in the Wasiriya Beds and that Lake Victoria was smaller, contracted

from a climate more arid than the modern, thus Rusinga Island was continuous with the mainland. Tucker and Slingerland (1997)'s model would predict that punctuated rain events after a long dry hiatus likely deposited the graded-bedding, the massive poorly-sorted facies, the tuffaceous silt paleosol, and capping dark clayey paleosol. At the base of AV1006, the tufa deposit is overlain by ~1 m of poorly sorted mud, sand, and gravel, followed by a 2.5 m wide channel conglomerate with >20 cm cobbles, overlain by a succession of tuffaceous silt. This I interpret as an interval that was initially set in a spring-supported paleoenvironment. This was followed by a pulse of sedimentation from concentrating hillslope regolith at the valley bottom yielding the mud, sand, and gravel deposit that overlies the tufa. Eventually sediment-supply was exhausted and channel incisement progressed up-dip from drainage terminus, producing the comparatively large 2.5 m wide channel conglomerate, which was followed by tuff airfall and axial concentration.

The graded-bedding and laterally equivalent facies signify a very sudden increase in rain that punctuated a lengthy dry spell during which a mantle of regolith accumulated over the hillslopes of the Nyamita valley. Consistent with Tucker and Slingerland (1997) the manganese oxide staining in the graded-beds likely resulted from denuded and dissolved plant and other organic matter from upslope that was deposited with this sediment (Mount and Cohen, 1984).

Obviously the tuffaceous silt paleosol does not likely represent punctuated redeposition of hillslope regolith but rather punctuated redeposition of extrabasinal eolian volcanic silt. This sudden influx of sediment, during a time of comparatively low sediment-availability, essentially acts as a photo-plate inserted at a random time, a

passive substrate inserted to record a setting that would scarcely otherwise be geologically preserved and studied.

The presence of multiple widespread tuffs suggests remote volcanic control on the formation of the Wasiriya Beds is as important as climate. The dark capping clayey paleosol deposits also may have ultimately originated as airfall tuff and were perhaps intensely devitrified after deposition. This hypothesis requires further investigation. Both the tuffaceous and dark capping clayey paleosols rest 5-10 m above the modern axial drainage, contain abundant calcium carbonate precipitates and pedogenic features, suggesting that preserved deposits of these facies are indicative of channel terraces following aggradational events/phases, and that these terraces were hydrologically contiguous with a source of soluble calcium carbonate. The channel conglomerates contained within these facies indicate that colluvial silt and clay deposition was followed by an incisement phase. Tucker and Slingerland (1997) point out that the incisement could have occurred as soon as within a year of the punctuated silt and clay deposition. Nevertheless, the factors that contribute to obliteration of silt and clay deposits did not converge upon those deposits that remain today, and this may be attributable to a geologically-instantaneous confluence of many variables that are not precisely measurable (exact paleotopography, sediment supply, vegetation, climate, etc.).

The setting recorded by both the tuffaceous silt paleosol and the capping dark clayey paleosol is a stable landscape with active plant rooting and animal burrowing, at a time when rain was frequent enough to cause many fluctuations in water table height. Based on lithology and fabric, the tuffaceous silt was likely subaerially exposed less and less pedogenically modified than the capping, dark, clayey, more mature paleosol.

Though the clayey paleosol is pervasively stained with Mn-oxides, this may signify a brief punctuated denudation event in an otherwise undistinguished paleoenvironment, biasing the corresponding geological record. Due to potentially inconsistent geological preservation the relative duration and intensities of arid versus humid paleoenvironmental conditions are not necessarily accurately represented in the Wasiriya Beds. For instance, it is possible that the calcium carbonate cements and rhizoliths in the paleosol represent wetness and humidity that was a minority component of an overall arid period. A distinctly humid-climate facies is expected to reflect a substantially greater C3 vegetation $\delta^{13}C$ signature in pedogenic carbonate than other facies such as the tuffaceous silt paleosol.

What was not preserved is as important to consider as what is. What buried the tuffaceous silt paleosol and prevented it from becoming a mature paleosol? It may have just been the clayey paleosol, though it was never observed to directly cap the tuffaceous silt paleosol facies. If the widespread tuffaceous silt paleosol was deposited during an arid time period, then large amounts of regolith was being produced upslope in such an arid interval and may have blanketed the tuffaceous silt paleosol during a sudden intense rainstorm, only to later be stripped off the top of tuffaceous silt paleosol. Such a burial and re-exposure of the tuffaceous silt paleosol may be necessary to explain the wide range of dates derived from this pedogenically-immature facies. Overall, there is some uncertainty about how representative the studied Wasiriya Bed deposits are of their paleoenvironments, but future research could allay this uncertainty.

Regional Climate Inferred from the Wasiriya Beds

If East African climate is indeed coupled with glacial-interglacial cycles, then it would be more reasonable to predict that East African-LGM climate would be markedly dry. By ~26.5 ka, most ice sheets were at their maximum extent and sea-level was at a lowstand (Clark, 2009). The Wasiriya Beds fauna suggests a more arid climate than the modern (Faith et al., 2010). However the clayey paleosol facies suggests eastern Lake Victoria experienced relatively elevated humidity just prior to ~26-28 ka, which is just prior Last Glacial Maximum. Particularly clayey sediment such as this is expected to be generated by a longer duration of subaerial exposure than that probably experienced by the tuffaceous silt paleosol or from recording relatively elevated mean annual precipitation (MAP) but experiencing about as much subaerial exposure as the tuffaceous silt paleosol. It is important to characterize the origin of the clayey paleosol in order to characterize the mode of clay accumulation and possibly draw paleoclimatic inferences from it. If the high clay component derives from a distinct time period of heightened mean-annual precipitation, then it suggests some decoupling of tropical East African climate with high-latitude climate just prior to the Last Glacial Maximum. In other words the clayey paleosol deposits could contradict the assumption that increasing high-latitude glaciation prior to the LGM coincided with tropical aridity. However, the clayey paleosol may have developed due to a long duration of subaerial exposure rather than humidity penecontemporaneous with its corresponding gastropod dates. That the clayey paleosol indicates heightened humidity may concur with penecontemporaneous paleoclimate data from Lake Malawi (Cohen et al., 2007) and the Nile Delta (Revel et al., 2006), suggesting that East Africa did not experience a dramatically arid LGM. It was

only by about 17.2 ka, when the ice sheets began to recede, that extreme aridity apparently affected the Lake Victoria region (Johnson et al., 1996).

If the tufa deposits are manifestations of a relatively humid time period in the Lake Victoria region preceding deposition of the tuffaceous silt paleosol >45 ka, then it is possible that the tufa formed during the earlier humid period (60-50 ka) within the last glacial period as identified by Revel et al. (2010) 60-50 ka. Isotopic research on tufa laminations could clarify the paleoclimate associated with the tufa, unless the aquifer is independent of penecontemporaneous climate. It is reasonable to tentatively extend Revel et al. (2010)'s hypothesis about moisture distribution patterns in Ethiopia to the Lake Victoria region, considering that Randel and Johnson (1991) and Williams (1991) mapped volcanic ash distributions from the Eastern Rift and determined that the prevailing winds during the Late Pleistocene were south and west. Dating the tufa (perhaps by uranium-series methods) would be very useful in potentially reconstructing the history of the lower Wasiriya Beds and integrating the tufas with broader paleoenvironmental theories. Perhaps the graded bedding and its lateral poorly-sorted equivalent represent a relatively arid accumulation of hill-slope regolith that was followed by the influx of tuff by ~45 ka that became moderately pedogenically altered. Again, determining with some precision the age of the graded beds would be very helpful in reconstructing the timing of Wasiriya Beds deposition. The mid and upper Wasiriya Beds, the tuffaceous silt paleosol facies and the clayey paleosol facies dated from 45-26 ka appear to comprise a time interval that was semiarid until about 33 ka and then by as late as 28 ka the Rusinga Island region possibly became more humid with higher rates of chemical weathering.

Prediction of Archaeological Site Distribution

The lateral and vertical distributions of facies may bear important implications for the distribution of archaeological sites at Nyamita both spatially and temporally. One challenge in predicting the parameters of artifact deposition is that hominins can transport artifacts in defiance of gravity and thus work as agents of sedimentation that contradict fundamental sedimentologic assumptions. Some probabilistic predictive hypotheses have been proposed. There is evidence to suggest that a stable landscape surface is a more likely site for artifact manufacture, use, and discard than an unstable surface (Holliday, 2004; Tryon, 2010). Work by Deocampo et al. (2002) at Olduvai Gorge found a significant correlation between artifact abundance and clay mineralogy that is indicative of freshwater conditions, hence a proposed affinity of hominids and early humans for freshwater-body margin sites. At least two *in-situ* lithic artifacts (one somewhat rounded, one not) have been recovered from channel conglomerates at Nyamita, though it is not certain if artifacts have a significant affinity to channel conglomerates. If artifacts were discarded at an unstable point on the landscape at Nyamita they would be susceptible to colluviation and deposition in channel conglomerates during seasonal rain. Thus spatial and temporal variation of landscape stability at Nyamita has potential implications for archaeological site distribution. However, the weakness of this hypothesis is that hominins may be less likely to perform artifact-related activities on unstable parts of the landscape.

The stratigraphically lowest and oldest Wasiriya Bed deposits include tufas that indicate that Nyamita contained point sources of freshwater, which may have been attractive for animals and humans (Ashley et al., 2002). Far more information is needed to usefully characterize the tufa deposits at Nyamita and their associated

paleoenvironmental data before they can be integrated into hypothesis about hominin paleoenvironments.

The Nyamita valley axis probably contained patches of stable land surfaces that supported plant life and hosted burrowing animals, as the density of root traces in these deposits suggests that the valley bottom was wet for at least several weeks. In archaeological context, this aggrading valley bottom at Nyamita may have attracted many animals as well as humans since it at least sporadically contained water. The faunal and isotopic data suggesting local wetness in a regional open arid environment (Faith et al., 2010; Garrett et al., 2010; Tryon et al., 2010; Tryon et al., in press). The faunal evidence suggests Rusinga Island was part of the mainland and that lake level was perhaps lower than in the modern (Faith et al., 2010), or that the Mfangano fault has since been displaced. In paleoenvironmental context, the Nyamita valley bottom could have been a wet oasis in a vast arid open grassland. If the capping clayey paleosol does signal wet, vegetated, tuff-devitrifying conditions, then it suggests that hominins could find such a paleoenvironment comparatively hospitable during the LGM time-period that hypothetically corresponded with widespread aridity.

CHAPTER FIVE

Conclusions

This study provides a strong tephrostratigraphic framework to contextualize research in the Wasiriya Beds at Nyamita. This study did not encounter evidence supporting previous hypotheses that the Wasiriya Beds preserve lacustrine conditions, though the possibility remains. There is evidence to support recent inferences that the Rusinga Island in the Late Pleistocene was locally relatively in a broader arid grassland context. However, the extent to which sedimentary proxies for climate are generally representative of Rusinga Island's paleoenvironment is difficult to tell. The sporadic pacing of sedimentation I infer from the Wasiriya Beds suggests that very brief episodes of pluvial input had the most dramatic effects on the Late Pleistocene sedimentary record at Nyamita. The landscape was vegetated persistently, and abundant sedimentary mineral precipitates suggest sharply alternating wet and dry conditions, possibly seasonality. This study may support the hypothesis that East Africa was extremely arid just prior to the LGM if the graded bedding facies resulted from a lengthy and severe drought that led to high sediment yields from physical weathering in accordance with the valley-drainage model.

Some potentially revealing details about the Wasiriya Beds remain unknown, although this study established a basis for framing such future inquiries. Future research on the Wasiriya Beds at Nyamita should work toward elaborating on the geochronological and paleoenvironmental context of the tufa and graded-bedding deposits. The tufas and any overlooked wetland facies hold great potential for

contributing important paleoenvironmental context that could influence archaeological interpretation of hominin-environmental pressures.

APPENDICES

APPENDIX A

Table A.1 Raw elemental composition data of tuff sample electron microprobe grain analyses; in weight percent.

n	SiO_2	TiO_2	Al_2O_3	FeO	MnO	MgO	CaO	Na_2O	K_2O	Total
CAT09-05										
1	60.4	0.62	15.38	7.68	0.34	0.27	0.99	8.26	4.6	98.54
2	57.71	0.46	14.89	7.32	0.31	0.28	0.91	6.45	4.52	92.85
3	59.43	0.5	15.3	7.26	0.22	0.31	1	7.5	4.79	96.32
4	60.39	0.63	15.32	7.73	0.28	0.3	1.03	8.59	4.77	99.05
5	59.02	0.69	15.14	6.95	0.29	0.29	1	7.93	4.43	95.74
6	60.51	0.56	15.54	7.63	0.29	0.28	1.01	8.05	4.79	98.65
7	60.51	0.65	15.41	7.54	0.32	0.29	1.01	8.4	4.83	98.95
8	60.15	0.63	15.14	7.46	0.29	0.28	0.98	8.25	4.83	98.01
9	60.9	0.51	15.23	7.36	0.33	0.28	1.05	8.45	4.63	98.75
10	61.18	0.52	15.51	7.43	0.35	0.31	1.02	8.52	4.62	99.46
AV1004T5A										
1	66.7	0.53	11.31	8.11	0.3	0.13	0.7	6.72	4.63	99.14
2	64.16	0.44	10.63	7.66	0.37	0.11	0.64	6	4.34	94.34
3	64.01	0.44	10.73	7.61	0.29	0.1	0.64	5.59	4.38	93.79
4	63.67	0.58	10.76	7.72	0.3	0.1	0.6	5.67	4.35	93.75
5	63.93	0.6	10.86	7.63	0.32	0.12	0.69	5.87	4.44	94.44
6	63.66	0.52	10.75	7.85	0.32	0.09	0.57	5.66	4.35	93.78
7	64.95	0.6	10.91	7.51	0.27	0.11	0.66	6.25	4.39	95.65
8	63.8	0.51	10.91	7.65	0.25	0.11	0.63	5.85	4.35	94.06
9	66.16	0.63	11.07	8.03	0.26	0.11	0.67	6.66	4.65	98.25
10	63.96	0.61	10.75	7.57	0.34	0.12	0.65	5.98	4.3	94.29
AV1006B										
1	58.55	0.41	15.14	7.19	0.3	0.27	0.96	6.56	4.7	94.08
2	60.31	0.64	15.52	7.45	0.37	0.29	0.95	8.03	4.77	98.33
3	61.04	0.64	15.5	7.63	0.22	0.28	0.97	8.24	4.92	99.44
4	61.33	0.63	16.19	6	0.29	0.46	1.27	7.2	5.1	98.46
5	60.62	0.65	15.61	7.57	0.27	0.27	0.99	8.48	4.78	99.24
6	59.18	0.5	15.38	7.2	0.29	0.31	1	7.36	4.56	95.77
7	60.4	0.48	15.5	7.52	0.24	0.33	1.04	8.51	4.9	98.92
8	61.13	0.54	15.56	7.7	0.29	0.3	1.01	7.55	4.94	99.01
9	58.97	0.52	15.09	7.37	0.3	0.28	1.07	6.96	4.56	95.1
10	58.69	0.64	14.94	7.23	0.31	0.27	0.74	4.57	4.46	91.86
11	56.29	0.65	14.18	7.38	0.26	0.32	0.93	4.15	4.2	88.36
12	60.38	0.54	15.57	7.31	0.23	0.29	1.02	8.4	4.85	98.6
13	59.15	0.56	15.2	7.15	0.31	0.28	1.05	6.04	4.48	94.22

Table 1 Raw elemental composition data of tuff sample electron microprobe grain analyses; in weight percent - Continued.

n	SiO_2	TiO_2	Al_2O_3	FeO	MnO	MgO	CaO	Na_2O	K_2O	Total
AV1006D										
1	60.82	0.73	15.24	6	0.22	0.34	1.1	6.74	4.85	96.02
2	63.39	0.64	15.95	6.57	0.25	0.32	1.11	6.52	5.23	99.97
3	48.93	0.69	6.18	15.28	0.64	13.31	11.93	0.9	0.56	98.41
4	37.93	0.07	23.24	12.49	0.34	0.02	22.61	0	0	96.69
5	61.01	0.76	15.23	6.31	0.28	0.32	1.05	6.54	4.9	96.39
6	69.42	0.2	6.5	8.45	0.32	0.01	0.27	7.07	4.13	96.36
7	62.24	0.61	15.32	6.3	0.24	0.32	1.12	6.9	4.97	98.01
8	61.77	0.59	15.64	6.25	0.26	0.31	1.12	7.07	4.66	97.67
9	61.75	0.51	15.56	6.6	0.27	0.31	1.24	7	5.21	98.44
10	60.98	0.58	15.27	6.61	0.23	0.3	1.05	6.72	5.31	97.05
11	63.53	0.85	15.91	6.74	0.26	0.33	1.08	6.88	5.21	100.78
12	62.96	0.49	15.75	6.62	0.22	0.33	1.13	6.75	5.25	99.51
13	61.58	0.73	15.62	6.47	0.29	0.32	1.08	6.88	4.98	97.95
AV1002TA										
1	60.06	0.55	15.3	6.18	0.28	0.31	1.15	5.92	4.58	94.31
2	61.6	0.63	15.58	6.55	0.26	0.32	1.05	7	5.04	98.02
3	62.55	0.65	15.8	6.51	0.22	0.32	1.13	6.85	4.94	98.96
4	60.22	0.57	15.19	5.84	0.21	0.27	1.08	6.28	4.92	94.57
5	61.76	0.54	15.74	6.48	0.29	0.31	1.08	6.81	5.26	98.27
6	60.3	0.52	15.04	6.03	0.18	0.33	1.08	6.52	5.11	95.09
7	59.81	0.61	14.98	6.46	0.22	0.31	1.13	5.82	4.85	94.19
8	60.61	0.63	15.44	6.43	0.27	0.32	1.22	5.99	4.45	95.35
9	60.5	0.67	15.19	6.18	0.19	0.29	1.1	6.42	4.47	95.01
10	61.88	0.55	15.74	6.44	0.3	0.34	1.1	7.14	4.81	98.3
11	61.24	0.59	15.45	6.36	0.25	0.31	1.04	6.87	5.08	97.19
12	61.13	0.59	15.35	6.56	0.33	0.31	1.17	7.01	4.87	97.31
13	60.82	0.76	15.39	5.98	0.33	0.31	1.15	6.96	4.41	96.1
AV1004T3C										
1	60.53	0.54	15.21	6.25	0.21	0.35	1.12	6.38	4.84	95.42
2	60.42	0.64	15.37	6.23	0.32	0.3	1.2	6.56	4.7	95.73
3	61.37	0.79	15.36	6.24	0.19	0.3	1.17	3.53	4.49	93.43
4	60.62	0.57	15.51	6.06	0.29	0.34	1.16	6.74	5.04	96.31
5	60.67	0.63	15.33	6.41	0.3	0.29	1.14	6.96	5.02	96.74
6	61.35	0.57	15.74	6.33	0.22	0.3	1.05	7.15	4.45	97.16
7	59.06	0.58	14.69	5.66	0	0.28	1.09	3.74	4.67	89.78
8	62.94	0.5	15.89	6.58	0.27	0.33	1.11	7.3	5.28	100.2
9	61.31	1.32	15.89	7.3	0.24	0.72	1.64	6.87	4.54	99.82
10	62.98	0.67	15.96	6.22	0.26	0.31	1.13	7.24	4.85	99.6
11	62.96	0.5	15.59	6.59	0.2	0.35	1.17	7.13	4.95	99.43
12	62.27	0.52	15.66	6.36	0.18	0.35	1.16	7.12	5.25	98.87

Table 1 Raw elemental composition data of tuff sample electron microprobe grain analyses; in weight percent - Continued.

n	SiO_2	TiO_2	Al_2O_3	FeO	MnO	MgO	CaO	Na_2O	K_2O	Total
AV1004T3C (continued)										
13	61.53	0.5	15.47	6.35	0.24	0.32	1.1	7.16	4.66	97.33
AV1004T4C										
1	61.06	0.65	15.32	6.32	0.24	0.31	1.18	6.85	5.14	97.08
2	55.36	0.68	13.89	5.28	0.2	0.32	2	6.02	4.15	87.91
3	60.85	0.57	15.29	6.27	0.25	0.31	1.22	6.13	5.09	95.97
4	56.34	0.62	14.26	5.85	0.25	0.32	1.42	5.65	4.64	89.35
5	60.3	0.56	15.08	6.24	0.16	0.32	1.16	6.7	4.99	95.5
6	62.36	0.69	15.27	6.16	0.29	0.29	1.3	2.22	4.9	93.47
7	62.85	0.67	15.7	6.35	0.28	0.33	1.11	7.25	4.82	99.35
8	60.45	0.57	15.17	6.23	0.18	0.33	1.25	6.72	4.89	95.78
9	62.68	0.67	15.83	6.55	0.31	0.34	1.15	7.04	4.53	99.1
10	60.4	0.59	15.35	6.24	0.25	0.3	1.09	6.53	5	95.74
11	60.46	0.58	15.21	6.26	0.22	0.31	1.23	6.53	4.78	95.56
12	60.36	0.5	15.28	6.13	0.19	0.31	1.26	6.78	4.7	95.49
13	60.85	0.5	15.28	6.25	0.17	0.31	1.26	7.02	4.99	96.64
14	61.74	0.66	15.57	6.27	0.27	0.36	1.3	6.65	5.17	97.99
AV1004T5A										
1	64.96	0.68	10.79	7.45	0.25	0.1	0.67	6.18	4.53	95.62
2	65.34	0.62	10.97	7.91	0.33	0.1	0.63	6.44	4.58	96.93
3	64.93	0.52	10.76	7.84	0.24	0.13	0.67	6.62	4.47	96.17
4	64	0.59	10.74	7.31	0.26	0.11	0.67	5.7	4.46	93.82
5	63.89	0.68	10.53	7.47	0.28	0.11	0.63	4.27	4.29	92.14
6	66.77	0.57	11.03	7.71	0.37	0.09	0.73	6.32	4.61	98.19
7	65.74	0.44	11.07	8	0.26	0.1	0.65	6.6	4.48	97.34
8	65.11	0.41	10.27	7.98	0.27	0.1	0.62	6.38	4.47	95.59
AV1001T4										
1	61.84	0.57	15.28	6.45	0.2	0.29	1.06	7	4.82	97.51
2	61.87	0.6	15.53	5.98	0.24	0.25	0.89	7.22	4.87	97.46
3	62.19	0.64	15.83	6.43	0.25	0.32	1.11	7.19	5.19	99.15
4	59.83	0.54	15.09	6.18	0.21	0.28	1.02	6.6	4.48	94.25
5	60.44	0.59	15.36	6.23	0.29	0.31	1.12	6.74	4.93	96.01
6	63.5	0.59	15.92	6.58	0.31	0.31	1.16	6.75	4.79	99.92
7	61.15	0.67	15.31	6.38	0.16	0.3	1.13	6.58	4.96	96.65
8	60.66	0.59	15.34	6.17	0.26	0.33	1.07	6.23	5.08	95.74
9	67.31	0.11	18.82	0.61	0.01	0	0.17	7.48	6.39	100.91
10	60.97	0.74	15.31	6.2	0.2	0.31	1.21	6.53	5.16	96.63
11	60.32	0.53	15.25	6.39	0.32	0.27	1.01	6.57	4.8	95.46
12	60.99	0.7	15.38	6.66	0.29	0.34	1.15	6.91	4.61	97.02
13	60.16	0.69	15.12	6.17	0.22	0.32	1.37	5.7	4.93	94.67

Table 1 Raw elemental composition data of tuff sample electron microprobe grain analyses; in weight percent - Continued.

n	SiO_2	TiO_2	Al_2O_3	FeO	MnO	MgO	CaO	Na_2O	K_2O	Total
AV1003TB										
1	58.04	0.53	14.63	6.21	0.25	0.31	1.18	5.9	4.22	91.26
2	62.58	0.57	15.56	6.09	0.26	0.31	1.24	7.26	4.84	98.71
3	59.2	0.69	14.9	6.23	0.21	0.33	1.09	6.47	4.69	93.8
4	60.46	0.57	15.24	6.08	0.2	0.29	1.11	6.59	4.71	95.25
5	59.4	0.72	15.1	5.7	0.19	0.33	1.1	6.27	4.53	93.34
6	60.67	0.6	15.27	6.17	0.18	0.32	1.19	6.19	4.47	95.05
7	65.38	0.66	10.46	9.25	0.46	0.13	0.65	6.96	4.3	98.25
8	60.08	0.64	15.09	6.08	0.25	0.34	1.18	6.63	4.64	94.91
9	61.11	0.67	15.75	5.52	0.15	0.26	1.11	6.85	4.98	96.4
10	63.18	0.54	10.25	8.62	0.34	0.13	0.66	6.28	4.2	94.2
11	61.6	0.74	15.4	6.12	0.21	0.32	1.08	7.18	4.9	97.55
12	61.37	0.57	15.42	6.38	0.28	0.3	1.09	6.99	5.02	97.42
13	60.72	0.55	15.08	6.44	0.28	0.3	1.14	6.86	4.54	95.91
14	61.26	0.57	15.53	6.24	0.19	0.3	1.15	6.98	4.41	96.63

APPENDIX B

Table B.1 Section AV1001 description.

Height (cm)	Facies	Sample; Artifact	Height (cm)
0	Bedded Miocene rock		
100	Brown silty clay, moist with carbonate nodules	Sed/Ca 1	70
130	Polymictic conglomerate, (clasts 10-15cm) of granite, basalt, green lava in a matrix of cohesive brown silty clayey mud with very fine sand of quartz and medium sand-sized garnets, biotites, muscovites and carbonate nodules	Sed/Ca 2	110
170	Clayey to silty cohesive matrix of above with carbonate nodules and gravel lenses	Sed/Ca 3	160
230	Silty to sandy matrix of above with very course sand and gravel and carbonate nodules and gravel lenses of a loose consistency	Sed/Ca 4	220
490	The former facies grades upward into a brown silt to very fine sand, cohesive, with some clay content, carbonate nodules and gravel lenses with increasing calcareous lenses upward	Snail 1	430
250 to 430	Laterally 2 m to the west, the lithology grades into tuffaceous silt	Snail 2	450
410	Tuff is least reworked up-section where a gray (less devitrified) pocket was found	Sed/Ca 5	330
520	Conglomerate lens	Snail 3	350
670	Dark brown clay matrix at channel, clay matrix with some silt and fine sand and gravel clasts but lighter further from the gulley channel, carbonate nodules	Snail 4	380
		Tuff 1, Tuff 2	450
		Tuff 3	440
		Shells in Tuff	390-400

Table B.1 Section AV1001 description - Continued.

Height (cm)	Facies	Sample; Artifact	Height (cm)
		Tuff 4	370
		Snail 5	500
		Sed/Ca 6	500
		Snail 6	590
		Snail 7	610
		Sed/Ca 7	620

Figure B.1 AV1001 outcrop photograph; cows for scale.

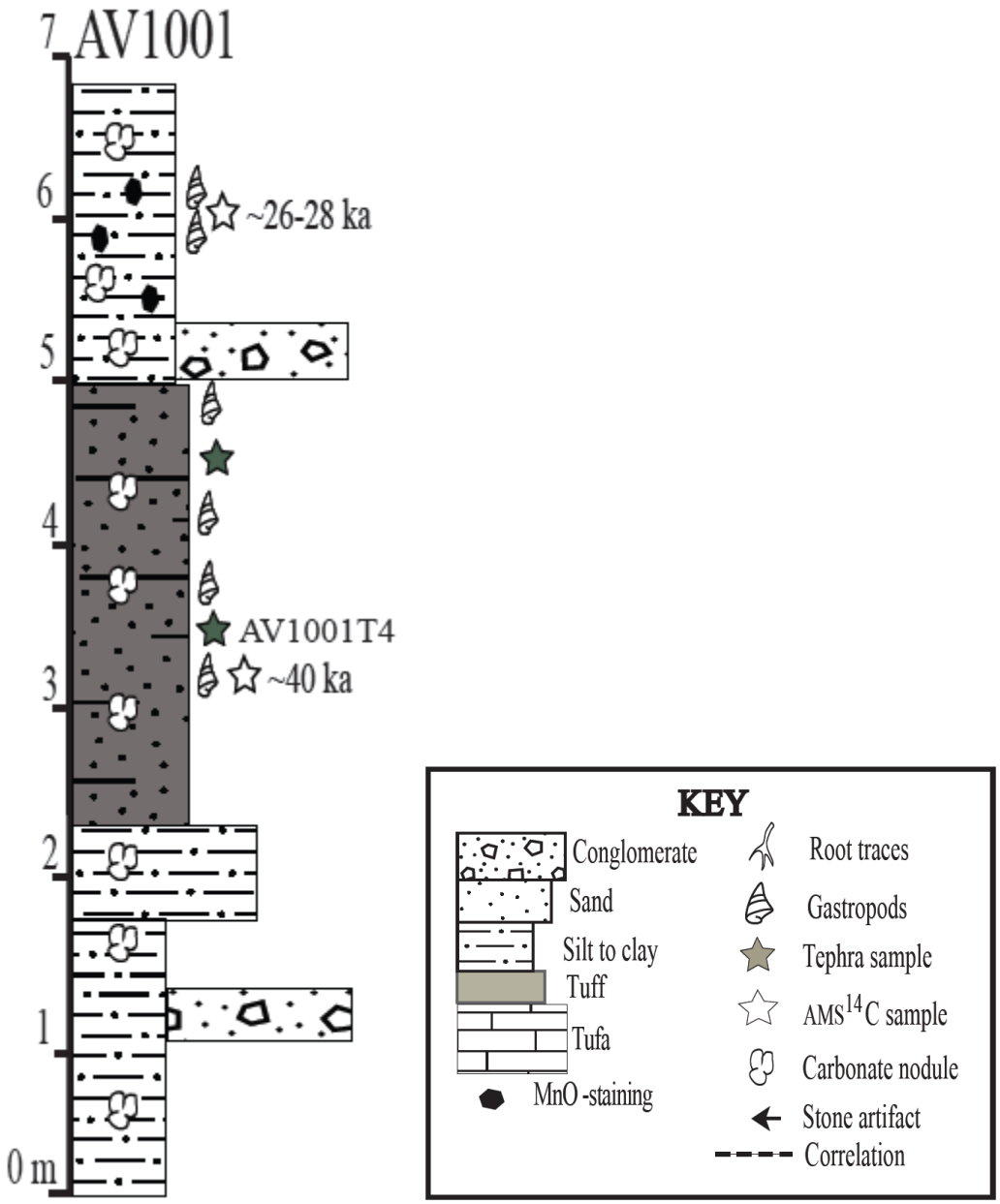

Figure B.2 AV1001 stratigraphic column and Legend to be referenced throughout Appendix B.

Table B.2 Section AV1002 description.

Height (cm)	Facies	Sample; Artifact	Height (cm)
0	Bedded Miocene rock		
0-240	(0629095, 9953989) Leg 1		
90	Silt and clay, brown matrix, gravel lenses, calcareous root casts, poorly sorted sand	Sed/Ca 1	50
150	Brown fine sand and silt matrix with lenses of poorly sorted fine to coarse sand, carbonate nodules, capped by calcrete	Ca 2	130
160	conglomerate cobbles 5-15 cm	Sed 2, Ca 3	170
200	Like the brown fine sand and silt facies in this section but as a succession, it is 20 cm mud, 5 cm poorly sorted sand/fine gravel, 1 cm fine garnetifferrous sand, 5 cm poorly sorted sand, 1cm mud, capped by calcrete (ground-water carbonate cemented sand and gravel)	Sed 3/ Ca 4	210
220	As preceding sediment, but with the fine sand interbedded with the gravel forming angled cross beds (fine sand is angles slightly and garnetiferous), brown muddy matrix, capped by a calcrete layer	Sed 7 (loose tuff), Tuff A, B, C, Snails 1, 2, 3, 4	220
240	Same as preceding (transition from leg 1 to leg 2 @ 240 cm)	Sed 4 Ca 5	350
190 - 320 cm	Laterally westward tuffaceous silt block-shaped deposit 15 m to the of the trenches has abundant calcareous root/burrow casts	Flake artifact	325
240-700	(0629087, 9953968) Leg 2		
460	Brown clay matrix with sand and gravel clasts, carbonate nodules, organic matter, matrix supported	Flake artifact	345
480	Conglomerate of polymict cobbles and gravel clasts, brown, silty matrix	Flake artifact	165
570	Brown, silty matrix gravel lenses, carbonate nodules, and grades up into… (Lat. grades from this facies to the succeeding facies)	Sed 5	470
700	As preceding, less gravel, darker color	Sed 6, Ca 6	570

Figure B.3 AV1002 outcrop; people in upper left for scale.

Figure B.4 Tuffaceous silt block.

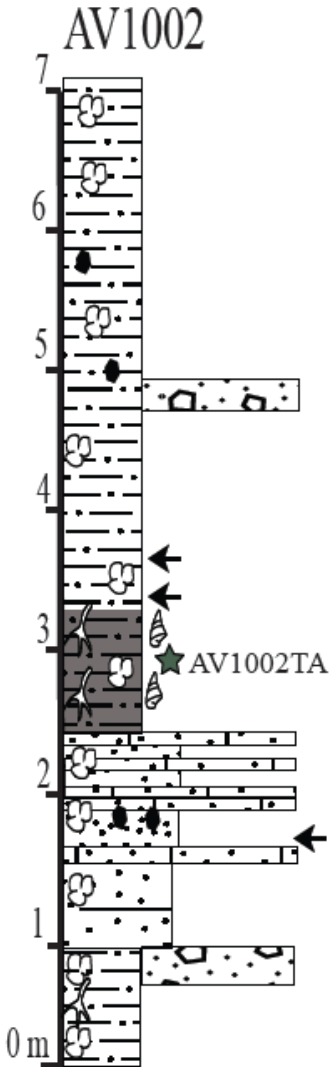

Figure B.5 AV1002 stratigraphic column.

Table B.3 Section AV1003 description.

Height (cm)	Facies	Sample; Artifact	Height (cm)
0	Bedded Miocene rock		
0-460	Leg 1		
190	Brown clay and silt matrix with sand and gravel clasts, angular breakage matrix supported	Sed/Ca 1	180
230	Poorly Sorted sand and gravel lenses at top of layer, garnetiferous	Sed/Ca 2	205
240	Calcrete layer: CaCO3-cemented sand and gravel	Sed/Ca 3	235
280	Polymict conglomerate 5-15 cm clasts in brown sand/silt matrix. Laterally appears lenticular with variable height and limited lateral continuity (contains Sed/Ca 4)	Sed/Ca 4	430
460	Loose, poorly sorted sand and gravel lenses in a brown silt matrix, much like AV1001 facies # 4. This darkens upward to 10YR 3/2	Sed/Ca 5	440
330-780	(0629059, 9953928) Leg 2	Snail 1	480
330-450	The preceding facies grades northward, following the gulley wall, to sandy brown clay	Tuff B	540
780	tuffaceous light brown silt, carbonate nodules, grading up into:	(0629060, 9953922) Tuff A	600
780-950	(0629069, 9953923) Leg 3: Darker Calcareous sandy silt with matrix-supported sand and gravel, calcareous nodules and root casts throughout, especially at the top	Sed/Ca 6	590
		Sed/Ca 7	730
		Sed/Ca 8	930

Figure B.6 AV1003 outcrop photographs; person is 1.8 m tall; the arrow points to the same tuffaceous silt unit in both pictures.

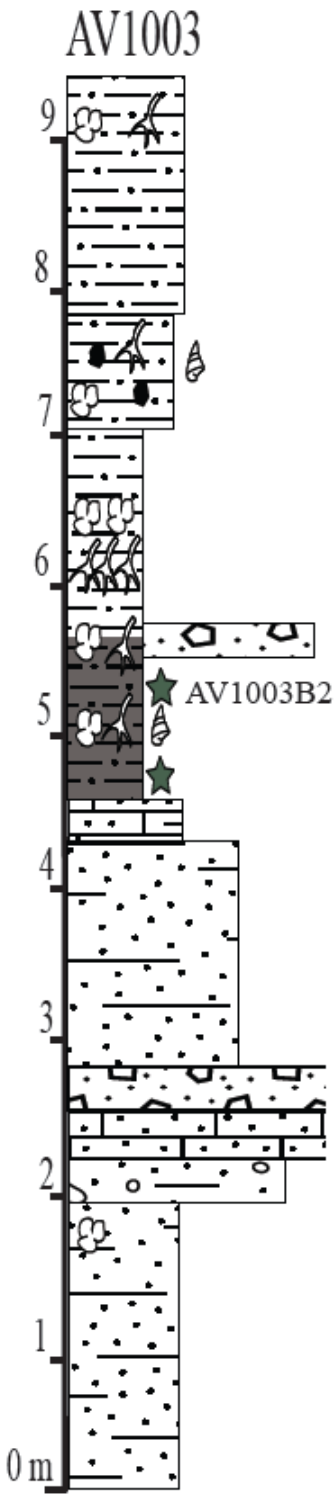

Figure B.7 AV1003 stratigraphic column.

Table B.4 Section AV1004 description.

Height (cm)	Facies	Sample; Artifact	Height (cm)
0	Miocene rock; possible Pleistocene calcrete, rhizoliths		
0-245	(0629025, 9953853) Section and Leg 1 base	Sed/Ca 1	10
20	Brown tuffaceous silt matrix, conglomerate and poorly sorted sand	Sed/Ca 2	40
50	Light cream-colored tuffaceous silt with CaCO3 nodules	Tuff 5	85
80-90	(0629027, 9953848) 2 m south of tuffaceous silt block, gray tuffaceous silt lens	Sed/Ca 3	110
110	Brown silt, poorly sorted sand, gravel (5-10 cm) polymictic conglomerate	Sed/Ca 4, Tuff 1	150
140	Brown silt, coarse sand, gravel lenses, grades up into:	Sed/Ca 5	160
160	Conglomerate	Tuff 2a, 2b	170
190	Brown matrix-supported tuffaceous silt and some gravel and sand, carbonate nodules	Sed/Ca 6, Tuff 3a, b, c (tuff block)	190-195
200	Light, Cleaner tuffaceous silt with gravel lenses, root casts, carbonate nodules and gray ash lenses at bottom (190cm)	Tuff 3d	195-200
210	Polymictic gravel conglomerate lenses laterally and vertically contacting calcrete lenses	Sed/Ca 7, Tuff 3e	200
240	Cream-colored tuffaceous silt with gravel lenses and carbonate root casts/nodules		
245	Cap on tuff block - is a very calcareous root mat/burrow complex	Sed/Ca 8, Tuff 3f	235-245
220-300	(0629034, 9953854) Leg 2		
240	Grain-supported poorly sorted sand, gravel, silt matrix		
260	Brown silty clay matrix, matrix-supported poorly sorted sand and gravel with carbonate nodules	Sed/Ca 9	270
280	Calcareous gravel/cobble conglomerate	Tuff 4a	290

Table B.4 Section AV1004 description - Continued.

Height (cm)	Facies	Sample; Artifact	Height (cm)
300	Brown silty clay matrix, matrix-supported poorly sorted sand and gravel with carbonate nodules	Tuff 4c (right block)	310
260-320	(0629035, 9953845) 15 m south of trenches, tuffaceous silt outcropping	Sed/Ca 10, Tuff 4d	360
300-410	Leg 3 (0629038, 9953847) light tuffaceous silt outcropping with carbonate nodules and root casts, alternating in succession, light and dark	Tuff 4b	330
310 to 650, trench top	Leg 4 (0629044, 9953838): dark clay, matrix-supported and poorly sorted sand with carbonate nodules, root casts and snail shells (decreasing upward)	Snails 1,2,3,4,5,6,7, Sed/Ca 11	330
		Snail 8	440
		Tuff 4e	490
		Sed/Ca 12	590

Figure B.8 AV1004 outcrop and tuffaceous silt block.

Figure B.9 A tuffaceous silt block to the right of view, part of the AV1004 measured section, trenched on the left.

Figure B.10 Clay paleosol capping section AV1004, person is 1.8 m tall.

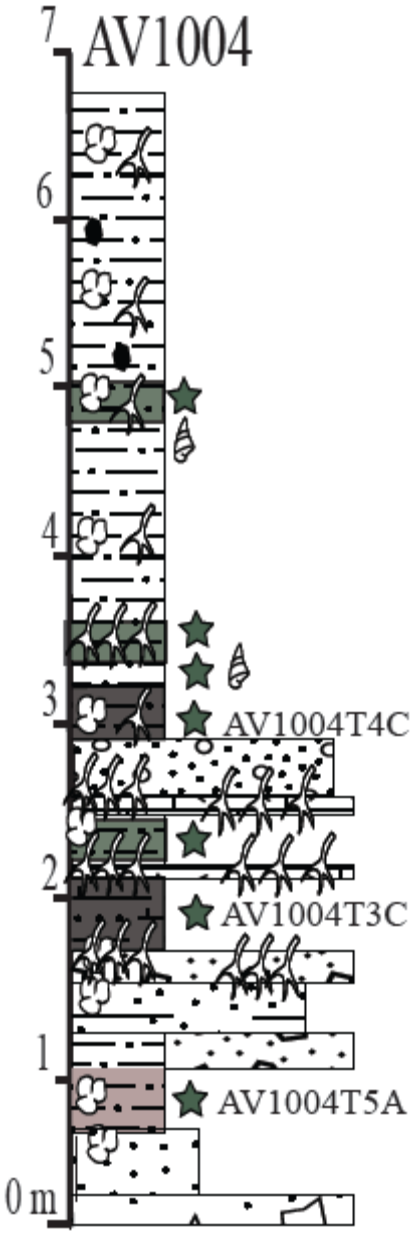

Figure B.11 AV1004 stratigraphic column.

Table B.5 Section AV1006 description.

Height (cm)	Facies	Sample/Artifact	Height (cm)
0	Miocene indurated braided-gravel rock		
0-370	(0628902, 9953104) Leg 1		
40	Brown silt and sand matrix with gravel and carbonate nodules	Sed/Ca 0	10
120	Tufa deposit, 2-3 m exposed	Sample CAT-10-15	
190	gravel/sand lenses, brown silt matrix	Sed/Ca 1	130
230	dark brown silty matrix, sand carbonate nodules, grades into, crosscut by a gravel bed (5-50 cm clasts)	Sed/Ca 2	200
370	light brown tuffaceous silt, with carbonate nodules	Sed/Ca 3,Tuff A	240
		Sed/Ca 4 Tuff B	310
510-520	Dipping conglomerate lens		
670	(0628917, 9953160) Leg 2	Tuff C	360
390-530	brown tuffaceous silt		
670	Tuff block of brown tuffaceous silt, root casts (burrows?), carbonate nodules, blocky peds	Sed/Ca 5, Tuff D	590
670-1680	(0628914, 9953212) Leg 3, uphill, across a stream channel and past Miocene outcrops		
780	Tuffaceous silt block, light brown tuffaceous silt; laterally southward gradationally transitions to darker brown sandy and gravelly silt, carbonate nodules and root casts	Tuff E	770
1020	(0628920, 9953311) Tuffaceous silt with conglomerate lenses, root casts, carbonate nodules	Tuff G Sed/Ca 7, Tuff H, Sed/Ca 8	1020
1160	(0628896, 9953288) dark brown silt and clay with gravel and coarse sand conglomerate lenses; conglomerate lens at 1090 cm	Tuff F, Sed/Ca 6	1080
1680	(0629020, 9953363) Vehicle parking area: reworked clay, silt, sand, gravel lenses,		

Figure B.12 View of the tufa at the base of AV1006.

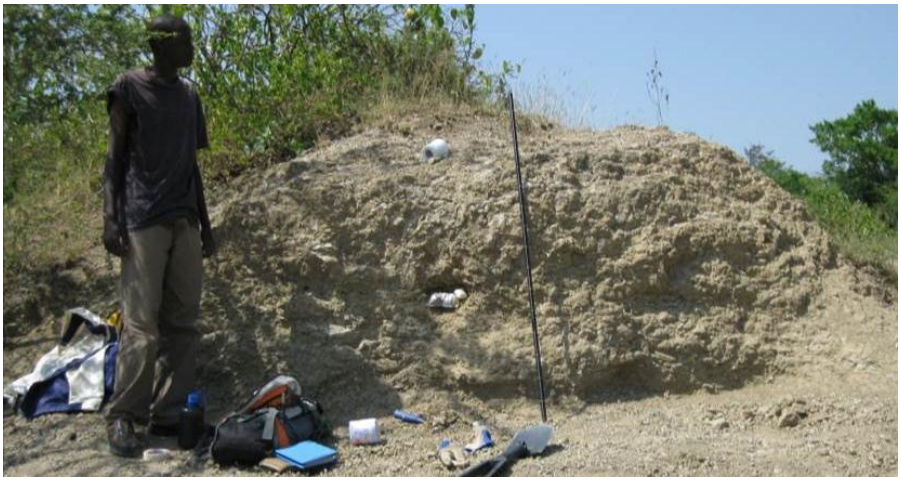

Figure B.13 View of the tuffaceous silt block in AV1006.

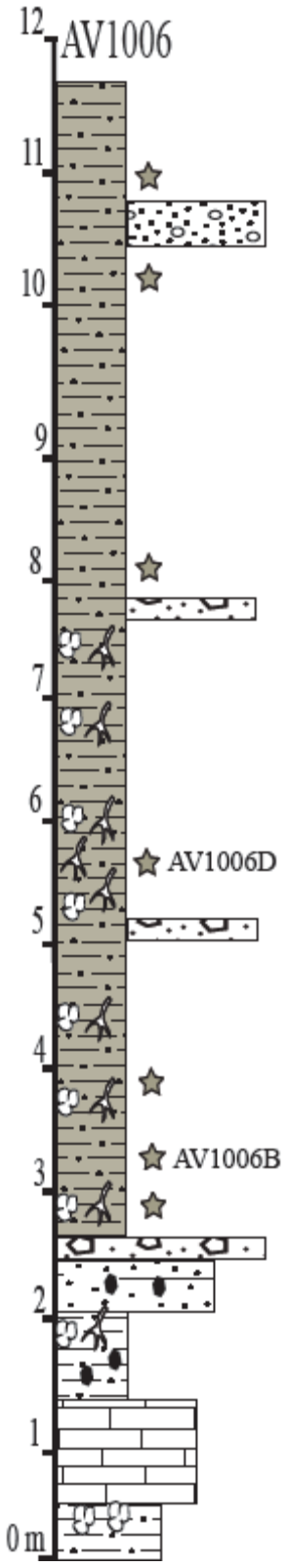

Figure B.14 AV1006 stratigraphic column.

Table B.6 Section AV1008 description.

Height cm	Facies	Sample; Artifact	Height (cm)
	Small tufa140-70 cm beneath base of Nyamita 1	CAT-10-14	100 cm below Nyamita 1
0	Miocene rock dipping north		0
60	Light brown calcareous sandy silty claystone with gravel lenses and carbonate nodules	Sed/Ca 1	60
110	Like the preceding sediment, except sandier and darker matrix	Sed/Ca 2	110
170	Like the preceding sediment.	Sed/Ca 3	170
180	Conglomerate lens		180
310	Lenses of mud to fine sand in a brown clay matrix	Sed/Ca 4	210
350	(approximate level of *in situ* artifacts)	Sed/Ca 5	260
370	Top of section	Sed/Ca 6	310
1120	Brown sandy silt with conglomerate lenses and carbonate nodules, conglomerate lens at 710-720		
1080-1120	Extensive gravel lag		

Figure B.15 View of the basal Miocene-Pleistocene contact of AV1008.

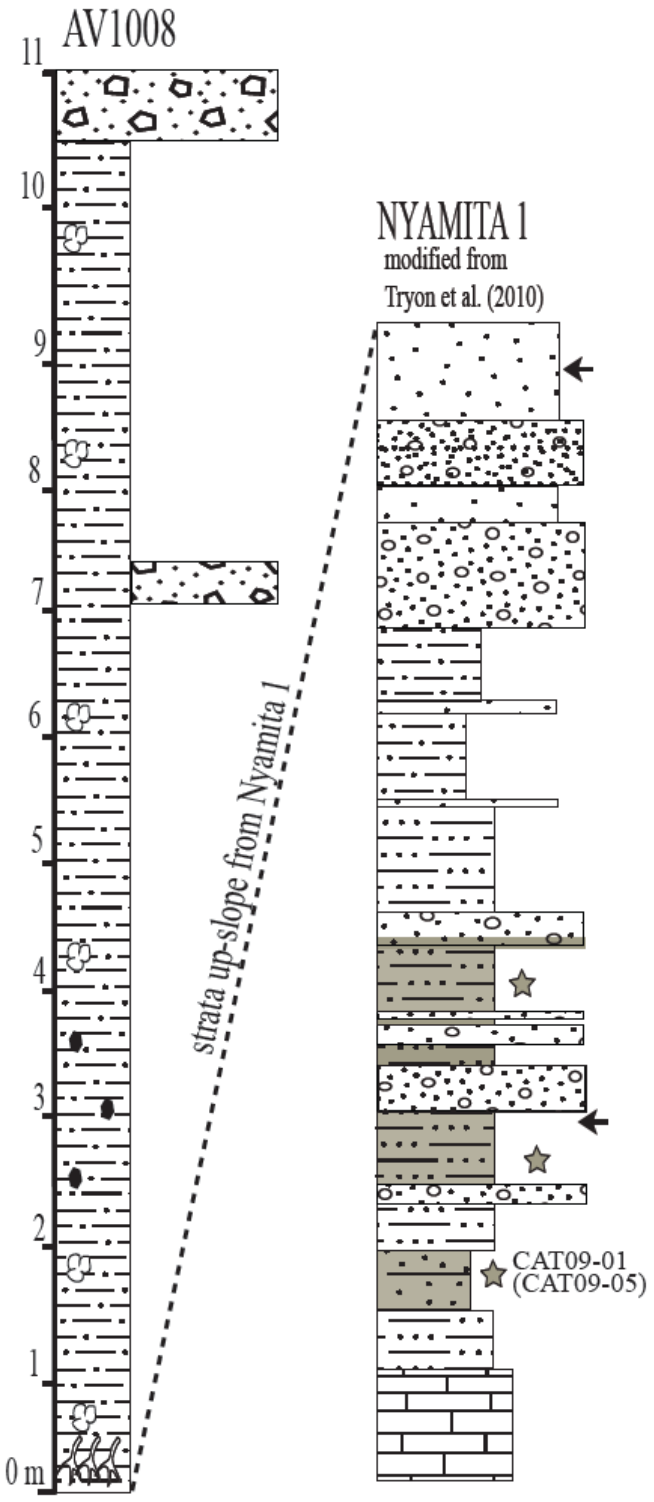

Figure B.16 AV1008 measured section.

Table B.7 Euclidean distance values.

Sample	AV1001T4	AV1002TA	AV1003TB2	AV1004T3C	AV1004T4C	AV1004T5A	AV1006B	AV1006D	CAT09-05
AV1001T4	0								
AV1002TA	4	0							
AV1003TB2	23	29	0						
AV1004T3C	41	62	29	0					
AV1004T4C	5	15	21	29	0				
AV1004T5A	3223	3208	3229	3589	3259	0			
AV1006B	320	369	234	177	285	3821	0		
AV1006D	28	51	62	28	23	3481	287	0	
CAT09-05	870	954	702	605	805	4288	146	793	0

WORKS CITED

Ambrose, S.H., Lorenz, K.G. 1990. Social and ecological models for the Middle Stone Age in southern Africa. In: Mellars, P. (Ed.), *The Emergence of Modern Humans: An Archaeological Perspective*. Edinburgh University Press, Edinburgh, p. 3-33.

Andrews, J. 2005. Paleoclimatic records from stable isotopes in riverine tufas: Synthesis and review. *Earth-Science Reviews*, 75, p. 85-104

Ashley, G.M., Goman, M., Hover, V.C., Owen, R. B., Renaut, R.W., Muasya, A.M. 2002. Artesian blister wetlands, a perennial water resource in the semi-arid Rift Valley of East Africa. *Wetlands*, vol. 22, no. 4, p. 686-695.

Banks, W.E., d'Errico, F., Dibble, H.L., Krishtalka, L., West, D., Olszewski, D.I., Peterson, A.T., Anderson, D.G., Gillam, J.C., Montet-White, A., Crucifix, M., Marean, C.W., Sánchez-Gõni, M.-F., Wohlfarth, B., Vanhaeran, M. 2006. Ecocultural niche modeling: new tools for reconstructing the geography and ecology of past human populations. *PaleoAnthropology*, p. 68-83.

Barham, L., Mitchell, P. 2008. *The First Africans: African Archaeology from the Earliest Toolmakers to most Recent Foragers.* Cambridge University Press, Cambridge.

Beaty, C. 1959. Slope retreat by gullying. *Geological Society of America Bulletin*, v. 70, no. 11, p. 1479.

Behar, D.M., Villems, R., Soodyall, H., Blue-Smith, J., Pereira, L., Metspalu, E., Scozzari, R., Makkan, H., Tzur, S., Comas, D., Bertranpetit, J., Quintana-Murci, L., Tyler-Smith, C., Wells, R.S., Rosset, S. 2008. The Dawn of Human Matrilineal Diversity. *The American Journal of Human Genetics*, 82, p. 1130-1140.

Basell, L. 2008. Middle Stone Age (MSA) site distributions in eastern Africa and their relationship to Quaternary environmental change, refugia and evolution of Homo sapiens. *Quaternary Science Reviews*, 27, p. 2484-2498.

Bertran, P., Hetu, B., Texier, J., Van Steijn, H. 1997. Fabric characteristics of subaerial slop deposits. *Sedimentology*, 44, p. 1-16.

Beuning, K.M., Kelts, K., Ito, E., Johnson, T. C. 1997. Paleohydrology of Lake Victoria, East Africa, inferred from 18O/16O ratios in sediment cellulose. *Geology*, December, vol. 25, no. 12, p. 1083-1086.

Beuning, K.M., Kelt, K., Russell, J., Wolfe, B. B. 2002. Reassessment of Lake Victoria-Upper Nile River paleohydrology from oxygen isotope records of lake-sediment cellulose. *Geology*, June, vol. 30, no. 6, p. 559-562.

Bishop, W.W. 1966. Stratigraphical geomorphology: a review of some East African landforms. In: Drury, G. H. (ed.), *Essays in Geomorphology*, p. 139-176. Heinemann, London.

Bishop, W.W. and Trendall, A F. 1967. Erosion surfaces, tectonics and volcanic activity in Uganda. *Quarternary Journal of the Geological Society of London*, 122, p. 385–420.

Bock, M., Schmitt, J., Möller, L., Spahni, R., Blunier, T. & Fischer, H. 2010. Hydrogen isotopes preclude marine hydrate CH4 emissions at the onset of Dansgaard-Oeschger events. *Science*, 328, p. 1686.

Broecker, W.S. 2003. Does the trigger for abrupt climate change reside in the ocean or in the atmosphere? *Science*, vol. 300, June, L20702.

Brown, F., Harris, J., Leakey, R., Walker, A. 1985. Early Homo erectus skeleton from west Lake Turkana, Kenya. *Nature*, vol. 316, 29 August.

Brown, F.H., Haileab, B., and McDougall, I. 2006, Sequence of tuffs between the KBS Tuff and the Chari Tuff in the Turkana Basin, Kenya and Ethiopia. *Journal of the Geological Society of London*, v. 163, p. 185–204.

Brown, E.T., Johnson, T.C., Scholz, C.A., Cohen, A.S., King, J.W. 2007. Abrupt change in tropical African climate liked to the bipolar seesaw over the past 55,000 years. *Geophysical Research Letters*, vol. 34,

Byerly, G.R., Melson, W.G., Nelen, J., and Jarosewich, E. 1977. Abyssal basaltic glasses as indicators of magma compositions. *Smithsonian Contributions to the Earth Sciences*, 19:22-30.

Campisano, C., Feibel, C. 2008. Tephrostratigraphy of the Hadar and Busidima Formations at Hadar, Afar Depression, Ethiopia. *The Geological Society of America, Special Paper* 446.

Clark, P.U. 2009. The Last Glacial Maximum. *Science*, 325, 710.

Cerling, T., Brown, F.H., Bowman, J. 1985. Low-temperature alteration of volcanic glass: hydration, Na, K, 18O and Ar mobility. *Chemical Geology (Isotope Geoscience Section)*, 52, 281-293.

Clement, A.C., Cane, M.A., and Seager, R. 2001. An orbitally driven tropical source for abrupt climate change. *Journal of Climate*, 14, 2369– 2375.

Clement, A.C., Hall, A., Broccoli, A.J. 2004. The importance of precessional signals in the tropical climate. *Climate Dynamics*, 22: 327-341.

Cohen, A.S., Stone, J.R., Beuning, K.R.M., Park, L.E., Reinthal, P.N., Dettman, D., Scholz, C.A., Johnson, T.C., King, J.W., Talbot, M.R., Brown, E.T., Ivory, S.J. 2007. Ecological consequences of early Late Pleistocene megadroughts in tropical Africa. *Proceedings of the National Academy of Science*, 104, p. 16422-16427.

Crevecoeur, I., Rougier, H., Grine, F., Froment, A. 2009. Modern human cranial diversity in the Late Pleistocene of Africa and Eurasia: evidence from Nazlet Khater, Pes¸tera cu Oase, and Hofmeyr. *American Journal of Physical Anthropology*. 140, p. 347-358.

De la Fuente, S., Cuadros, J., Fiore, S., Linares, J. 2000. Electron microscopy study of volcanic tuff alteration to illite-smectite under hydrothermal conditions. *Clays and Clay Minerals*, vol. 48, no. 3, p. 339-350.

DeMenocal, P. 2004. African climate change and faunal evolution during the Pliocene-Pleistocene. Earth and Planetary Science Letters, 220, p. 3-24.

Denton, J.S. and Pearce, N.J. 2008. Comment on "A synchronized dating of three Greenland ice cores throughout the Holocene" by B.M. Vinther et al.: No Minoan tephra in the 1642 B.C. layer of the GRIP core. *Journal of Geophysical Research*, 113: D04303.

Deocampo D.M., Blumenschine R.J. and Ashley G.M. 2002. Wetland diagenesis and traces of early hominids, Olduvai Gorge, Tanzania. *Quaternary Research*, 57: 271–281.

Din, N.A. 1971. Observations on reproduction, aestivation and polymorphism in the snail *Limicolaria martensiana* (Smith) from the Queen Elizabeth National Park, Uganda. *Journal East African Natural History Society National Museum*, 29, 1-3.

Doornkamp, J.C. and Temple, P.H. 1966. Surface, drainage and tectonic instability in part of southern Uganda. *Geographic Journal*, 132: 238-252.

Eerkens, J.W., Lipo, C.P. 2005. Cultural transmission, copying errors, and the generation of variation in material culture and the archaeological record. *Journal of Anthropology and Archaeology*, 24, p. 316-334.

Faith, J.T., Choiniere, J., Tryon, C., Peppe, J., Fox, D. 2010. Taxonomic status and paleoecology of *Rusingoryx atopocranion* (Mammalia, Artiodactyla), an extinct Pleistocene bovid from Rusinga Island, Kenya. *Quaternary Research*, in press.

Feibel, C. 1999. Tephrostratigraphy and Geological Context in Paleoanthropology. *Evolutionary Anthropology*, vol. 8, no. 8, p. 87-100.

Flohn, H. and Burkhardt, T. 1985. Nile Runoff at Aswan and Lake Victoria: A Case of a Discontinuous Climate Time Series. *Z. Gletscherk. Glazialgeol*. 21, p. 125–130.

Froggatt, P. C. 1992. Standardization of the chemical analysis of tephra deposits. Report of the ICCT Working Group. *Quaternary International*, 13/14: 93-96.

Fuente, S., Cuadros, J., Fiore, S., Linares, J. 2000. Electron microscopy study of volcanic tuff alteration to illite-smectite under hydrothermal conditions. Clays and Minerals, Vol. 48, No. 3, 339-350.

Garcin, Y. 2008. Comment on ‘‘Abrupt change in tropical African climate linked to the bipolar seesaw over the last 55,000 years’’ by E. T. Brown, T. C. Johnson, C. A. Scholz, A. S. Cohen, and J. W. King, *Geophysical Research Letters*, 35.

Garret, N., Fox, D., McNulty, K., Tryon, C., Peppe, D. 2010. Isotope paleoecology of the Pleistocene Wasiriya Beds of Rusinga Island, Kenya. *Journal of Vertebrate Paleontology*, SVP Program and Abstracts Book 2010, 94A.

Goodfriend, G.A. 1987. Radiocarbon age anomalies in shell carbonate of land snails from semi-arid areas. *Radiocarbon,* 29: 159-167.

Goodfriend, G.A. and Stipp, J.J. 1983. Limestone and the problem of radiocarbon dating of land-snail shell carbonate. *Geology,* 11: 575-577.

Grine, F. E., Bailey, R. M., Harvati, K., Nathan, R. P., Morris, A. G., Henderson, G. M., Ribot, I., Pike, A. W. G. 2007. Late Pleistocene human skull from Hofmeyr, South Africa, and modern human origins. *Science*, vol. 315, 226.

Gutierrez-Castorena, M., Ortiz-Solorio, C., Sanchez-Guzman, P. 2007. Clay coatings formation in tepetates from Texcoco, Mexico. Catena, 71, p. 411-424.

Gunz, P., Bookstein, F.L., Mitteroecker, P., Stadlmayr, A., Seidler, H., Weber, G.W. 2009. Early modern human diversity suggests subdivided population structure and a complex out-of-Africa scenario. *Proceedings of the National Academy of Science,* 106, p. 6094-6098.

Harvey, A. 1989. The occurrence and role of arid zone alluvial fans. In: Thomas, D., ed. *Arid Zone Geomorphology,* Belhaven Press, a division of Pinter Publishers London.

Hay, R.L. 1968. Chert and its sodium-silicate precursors in sodium-carbonate lakes of East Africa. *Contributions to Mineralogy and Petrology*, 17: 255-274.

Haynes, C.V., Mead, A.R. 1987. Radiocarbon dating and paleoclimatic significance of subfossil *Limicolaria* in northwestern Sudan. *Quaternary Research*, 28, 86-99.

Henshilwood, C., Marean, C. 2003. The origin of modern human behavior. *Current Anthropology*, Volume 44, Number 5, December.

Hem, J. 1964. Deposition and solution of manganese oxides. *U.S. Geological Survey Water Supply*, Paper 1667-A, 64p.

Holliday, V.T. 2004. *Soils and Archaeological Research.* Oxford University Press, Oxford, UK.

Hopwood, Tindell. 1933. Miocene Primates from Kenya. *Journal of the Linnean Society of London, Zoology,* vol. 38, Issue 260, p. 437–464, November.

Howell, F.C. 1999. Paleo-demes, species clades, and extinctions in the Pleistocene hominin record. *Journal of Anthropological Research*. 55, 191-243.

Hunt, J., Hill, P. 1993. Tephra geochemistry: a discussion of some persistent analytical problems. *Holocene*, 3, 3, p. 271-278.

Jacobs, Z., Roberts, R.G., Galbraith, R.F., Deacon, H.J., Grun, R., Mackay, A., Mitchell, P., Vogelsang, R., Wadley, L. 2008. Ages for the Middle Stone Age of Southern Africa: implications for human behavior and dispersal. *Science,* 322, 733-735.

Jarosewich, E. 1979. Microprobe analyses of four natural glasses and one mineral: An interlaboratory study of precision and accuracy. *Smithsonian Contributions to the Earth Sciences*, 22:53-67.

Jarosewich, E., Nelson, J.A., Norbers, J.A. 1980. Reference samples for electron microprobe analysis. *Geostandards Newsletter*, 4:43-47.

Johanson, D., Masao, F., Eck, G., White, T., Walter, R., Kimbel, W., Asfaw, B., Manega, P., Ndessokia, P., Suwa, G. 1987. New partial skeleton of Homo habilis from Olduvai Gorge, Tansania. *Nature*, vol. 327, no. 6119, p. 205-209.

Johnson, T.C., Kelts, K., Odada, E. 2000. The Holocene History of Lake Victoria. *Ambio*, vol. 29, no. 1, Feb.

Johnson, T.C., Scholz, C.A., Talbot, M.R., Kelts, K., Ricketts, R.D., Ngobi, G., Beuning, K., Ssemmanda, I. and McGill, J.W. 1996. Late Pleistocene desiccation of Lake Victoria and rapid evolution of cichlid fishes. *Science,* 273: 1091-1093.

Jungers, W. 1982. Lucy's limbs: skeletal allometry and locomotion in *Australopithecus afarensis. Nature*, 297, p. 676 – 678, 24 June.

Kendall, R.L. 1969. An ecological history of the Lake Victoria basin. *Ecological Monographs*, 39: 121-176.

Kent, P.E. 1942. The country round the Kavirondo Gulf of Victoria Nyanza. *Geographical Journal*, 100: 22-31.

Kimbel, W., Johanson, D., Rak, Y. 1994. The first skull and other new discoveries of *Australopithecus afarensis* at Hadar, Ethiopia. *Nature*, vol. 368, p. 449-451, 31 March.

Klein, R. 2000. Archaeology and the evolution of human behavior. *Evolutionary Anthropology*, Articles, Wiley-Liss, Inc. p. 17-36.

Klein, R. 2009. *The Human Career: Human Biological and Cultural Origins, Third Edition*. University of Chicago Press.

Lahr, M.M., Foley, R. 1998. Towards a theory of modern human origins: geography, demography, and diversity in recent human evolution. Yearb. Phys. Anthropol., 41, p. 137-176.

Le Bas, M. 1977. *Carbonatite-nephelinite volcanism*. John Wiley & Sons ltd., Chichester and New York.

Le Bas, M., Le Maitre, R., Streckeisen, A., Zanettin, B. 1986. A chemical classification of volcanic rocks based on the total alkalai-silica diagram. *Journal of Petrology*, 27, 3, p. 745-750.

Leakey, L.S.B. 1948. Skull of Proconsul from Rusinga Island. *Nature,* London, vol. 162, p. 688.

Leuschner and Sirocko. 2003. Orbital insolation forcing of the Indian Monsoon – a motor for global climate changes? *Palaeogeography, Palaeoclimatology, Palaeoecology*, vol. 197, issues 1-2, p. 83-95.

Lofgren, G. 1971. Experimentally produced devitrification textures in natural rhyolitic glass. *GSA Bulletin*, vol. 82, no. 1, p. 111-124.

Lowe, D.J., Shane, P.A.R., Alloway, B., Newnham, R.M. 2008. Fingerprints and age models for widespread New Zealand tephra marker beds erupted since 30,000 years ago: a framework for NZ-INTIMATE. *Quaternary Science Reviews.* 27, p. 95-126.

Marean, C. 1992. Implications of late quaternary mammalian fauna from Lukenya Hill (South-Central Kenya) for paleoenvironmental change and faunal extinctions. *Quaternary Research*, 37, p. 239-255.

Marean, C., Gifford-Gonzalez, D. 1991. Late Quaternary extinct ungulates off East Africa and paleoenvironmental implications. *Letters to Nature*, vol. 351, 4 April.

Maslin, M.A., Trauth, M.H., 2009. Plio-Pleistocene east African pulsed climate variability and its influence on early human evolution, in "The first humans - Origins of the genus Homo". In: Grine, F.E., Leakey, R.E., Fleagle, J.G. (Eds.), *Vertebrate Paleobiology and Paleoanthropology Series*, Springer Verlag, p. 151-158.

Matsuoka, J., Kano, A., Oba, T., Watanabe, T., Sakai, S., Seto, K. 2001. Seasonal variation of stable isotopic compositions recorded in a laminated tufa, SW Japan. *Earth and Planetary Science Letters*, 192, p. 34–44.

McCall, G. S. 2006 Behavioral ecological models of lithic technological change during the later Middle Stone Age of South Africa. *Journal of Archaeological Science*, vol. 34, issue 10, p. 1738-1751.

McBrearty, S. 1981. Songhor: a Middle Stone Age site in western Kenya. *Quaternaria*, 23:171-190.

McBrearty, S. 1988. The Sangoan-Lupemban and Middle Stone Age sequence at the Muguruk site, western Kenya. *World Archaeology*, 19:379-420.

McBrearty, S., Brooks, A. 2000. The revolution that wasn't: a new interpretation of the origin of modern human behavior. *Journal of Human Evolution*. 39, p. 453-563.

McDougall, I., Brown, F.H., Fleagle, J.G. 2005. Stratigraphic placement and age of modern humans from Kibish, Ethiopia. *Nature*, 433, p. 733-736.

Mellars, P. 2006. Why did modern human populations disperse from Africa ca. 60,000 years ago? A new model. *Proceedings of the National Academy of Sciences*, 103, p. 9381-9386.

Morgan, L.E., Renne, P.R. 2008. Diachronous dawn of Africa's Middle Stone Age: new 40Ar/39Ar ages from the Ethiopian Rift. *Geology*, 36, p. 967–970.

Mount, J., Cohen, A. 1984. Petrology and geochemistry or rhizoliths from Plio-Pleistocene fluvial and marginal lacustrine deposits, East Lake Turkana, Kenya. *Journal of Sedimentary Petrology*, vol. 54, no. 1, March, 1984, p. 0263-0275.

Pearson, O.M. 2008. Statistical and biological definitions of "anatomically modern" humans: suggestions for a unified approach to modern morphology. *Evolutionary Anthropology*. 17, p. 38-48.

Pederson, J., Pazzaglia, F., Smith, G. 2000. Ancienct hillslope deposits: Missing links in the study of climate controls on sedimentation. Geology, January, vol. 28, no. 1, p. 27–30.

Pentecost, A. 2005. *Travertiene*. Springer, Netherlands.

Perkins, M., Nash, W., Brown, F., Fleck, R. 1995. Fallout tuffs of Trapper Creek, Idaho – A record of Miocene explosive volcanism in the Snake River Plain volcanic province. *GSA Bulletin*, December 1995, v. 107, no. 12, p. 1484 – 1506.

Pickford, M. 1984. Kenya Palaeontology Gazetteer, Western Kenya, Vol. 1. Nairobi, Kenya: National Museums of Kenya.

Pickford, M., Thomas, H., 1984. An aberrant new bovid (Mammalia) in subrecent deposits from Rusinga island, Kenya. *Proceedings Koninklijke Akademie des Wetenschappen*. B. 87, p. 441-452.

Pickford, M. 1995. Fossil land snails of East Africa and their paleoecological significance. *Journal of African Earth Sciences*, 20, p. 167-226.

Pickford, M. 1986. Cainozoic paleontological sites of Western Kenya. *Münchner Geowissenschaftlich Abhandlungen*, 8, p. 1-151.

Pollard, A. M., Blockley, S. P. and Lane, C. S. 2006. Some numerical considerations in the geochemical analysis of distal microtephra. *Applied Geochemistry*, 21: 1692-1714.

Potts, R. and Deino, A. 1995. Mid-Pleistocene change in large mammal faunas of East Africa. *Quaternary Research*, 43: 106-113.

Potts, R., 1998. Environmental hypotheses of hominin evolution. *Yearbook of Physical Anthropology*, 41, p. 93-136.

Pratt, D.J. and Gwynne, M.D. 1977. *Rangeland Management and Ecology in East Africa*. Hodder and Stoughton, London.

Quade, J., Wynn, J.G. (Eds.), 2008. The Geology of Early Humans in the Horn of Africa. *Geological Society of American Special Paper*, vol. 446, Boulder.

Randel, R.P., Johnson, R.W. 1991. Geology of the Suswa Area. Republic of Kenya Ministry of Environment and Natural Resources, Mines and Geological Department, Nairobi. Report No. 97.

Revel, M., Ducassou, E., Grousset, F. E., Bernasconi, S. M., Migeon, S., Revillon, S., Mascle, J., Murat, A., Zaragosi, S., and Bosch, D. 2010. 100,000 years of African monsoon variability recorded in sediments of the Nile margin. *Quaternary Science Reviews*, 29, p. 1342–1362.

Sarna-Wojcicki, S., 2000. Tephrochronology. In: Sowers, J.M., Lettis, W.R., Noller, J.S. (Eds.), Quaternary Geochronology: Methods and Applications. *American Geophysical Union*, Washington, DC, p. 357–377.

Scholz, C.A., Johnson, T.C., Cohen, A.S., King, J.W., Peck, J.A., Overpeck, J.T., Talbot, M.R., Brown, E.T., Kalindekafe, L., Amoako, P.Y.O., Lyons, R.P., Shanahan, T.M., Castañeda, I.S., Heil, C.W., Forman, S.L., McHargue, L.R., Beuning, K.R., Gomez, J., Pierson, J. 2007. East African megadroughts between 135 and 75 thousand years ago and bearing on early modern human origins. *Proceedings of the National Academy of Sciences*, 104, p. 16416-16421.

Semeniuk, V., and Meagher, T.D. 1981. Calcrete in Quaternary coastal dunes in Southwestern Australia: a capillary-rise phenomenon associated with plants. *Journal of Sedimentary Petrology*, vol. 41, p. 47-68.

Senut, B., Pickford, M., Gommery, D., Meind, P., Cheboie, K., Coppens, Y. 2001. First hominid from the Miocene (Lukeino Formation, Kenya)Premier hominidé du Miocène (formation de Lukeino, Kenya). *Earth and Planetary Science*, vol. 332, no. 2, 30 January, p. 137-144.

Sirocko, F. 2003. What drove past teleconnections? *Science*, 301, 1336–1337.

Smith, G. A. 1994. Climatic influences on continental deposition during late-stage filling of an extensional basing, southeastern Arizona. *GSA Bulletin* 106: 1212-1228.

Stager, J.C. and Johnson, T.C. 2008. The Late Pleistocene desiccation of Lake Victoria and the origin of its endemic fauna. *Hydrobiologia,* 596: 5-16.

Stager, J. C., Ryves, D. B., Chase, B. M., and Pausata, F. S. R. 2011. Catastrophic drought in the Afro-Asian monsoon region during Heinrich event 1. *Science*, 331, 1299.

Talbot, M.R. and Laerdal, T. 2000. The Late Pleistocene-Holocene paleolimnology of Lake Victoria, East Africa, based upon elemental and isotopic analyses of sedimentary organic matter. *Journal of Paleolimnology,* 23: 141-164.

Tierney, J.E. and Russell, J.M. 2007. Abrupt climate change in southeast tropical Africa influenced by Indian monsoon variability and ITCZ migration. *Geophysical Research Letters*, 34.

Tierney, J.E., Russell, J.M., Huang, Y., Sinninghe Damst´e, J.S., Hopmans, E.C., Cohen, A.S. 2008. Northern hemisphere controls on tropical southeast African, climate during the past 60,000 years. *Science,* 322, 252–255.

Tishkoff, S.A., Reed, F.A., Friedlaender, F.R., Christopher, E., Ranciaro, A., Froment, A., Hirbo, J.B., Awomoyi, A.A., Bodo, J.-M., Doumbo, O., Ibrahim, M., Juma, A.T., Kotze, M.J., Lema, G., Moore, J.H., Mortensen, H., Nyambo, T.B., Omar, S.A., Powell, K., Pretorius, G.S., Smith, M.W., Thera, M.A., Wambebe, C., Weber, J.L., Williams, S.M., 2009. The genetic structure and history of Africans and African Americans. *Science*, 324, 1035-1044.

Trauth, M.H., Deino, A., Strecker, M.R. 2001. Response of the East African climate to orbital forcing during the Last Interglacial (130-117 kyr BP) and the early Last Glacial (117-60 kyr BP). *Geology*, 29 (6), 499-502.

Trauth, M., Deino, A. L., Bergner, A. G. N., Strecker, M. R. 2003. East African climate change and orbital forcing during the last 175 kyr BP. *Earth and Planetary Science Letters*, 206, p. 297-313.

Trauth, M. H., Larrasoana, J. C, Mudelsee, M. 2009. Trends, rhythms, and events in Plio-Pleistocene African climate. *Quaternary Science Reviews*, 28, p. 399-411.

Trauth, M.H., Maslin, M.A., Deino, A., Junginger, A., Lesoloyia, M., Odada, E., Olago, D.O., Olaka, L., Strecker, M.R., Tiedemann, R. 2010. Human Evolution and Migration in a Variable Environment: The Amplifier Lakes of East Africa. *Quaternary Science Reviews*, 29, p. 2981-2988.

Tryon, C.A., McBrearty, S. 2006. Tephrostratigraphy of the Bedded Tuff Member (Kapthurin Formation, Kenya) and the nature of archaeological change in the later Middle Pleistocene. *Quaternary Research*, 65, p. 492–507.

Tryon, C., Logan, M., Mouralis, D., Kuhn, S., Slimak, L., Balkan-Atli, N. 2009. Building a tephrostratigraphic framework for the Paleolithic of Central Anatolia, Turkey. *Journal of Archaeological Science*, 36, p. 637-652.

Tryon, C. 2010. How the geological record affects our reconstructions of Middle Stone Age settlement patterns: The case of alluvial fans in Baringo, Kenya. In (N. Conard & A. Delagnes, eds.) *Settlement Dynamics of the Middle Paleolithic & Middle Stone Age, Volume III*. Tübingen: Kerns Verlag, pp. 39-66.

Tryon, C., Faith, J., Peppe, D., Fox, D., McNulty, K., Jenkins, K., Dunsworth, H., Harcourt-Smith, W. 2010. The Pleistocene archaeology and environments of the Wasiriya Beds, Rusinga Island, Kenya. Journal of Human Evolution, Volume 59, Issue 6, December 2010, Pages 657-671.

Tryon, C., Peppe, D., Faith, Van Plantinga, A., Nightingale, S., Ogondo, J., Fox, D. in press. Late Pleistocene artefacts and associated fauna from Rusinga and Mfangano islands, Lake Victoria, Kenya. *Azania*.

Tucker, G.E., Slingerland, R. 1997. Drainage basin response to climate change. *Water Resources Research*, vol. 33, no. 8, p. 2031-2047, August.

Van Couvering, J. 1972. *Geology of Rusinga Island and Correlation of the Kenya Mid-Tertiary Fauna*. Ph.D. Dissertation, Cambridge University.

Weninger, B., Jöris, O. 2008. A 14C age calibration curve for the last 60 ka: the Greenland-Hulu U/Th timescale and its impact on understanding the Middle to Upper Paleolithic transition in western Eurasia. *Journal of Human Evolution*, 55, p. 772-781.

White, T., Asfaw, B., Beyene, Y., Haile-Selassie, Y., Lovejoy, C.O., Suwa, G., WoldeGabriel, G. 2009. *Ardipithecus ramidus* and the Paleobiology of Early Hominids. *Science*, 2 October, vol. 326, no. 5949, p. 64, 75-86.

Williams, L.A.J. 1991. Geology of the Mau Area. Republic of Kenya Ministry of Environment and Natural Resources, Mines and Geological Department, Nairobi. Report No. 96.